Journal of Marine Science

Journal of Marine Science

Editor-in-Chief

Dr. Euge Victor Cristia RUSU

Contents

REVIEW

Roles of Geospatial Technologies in Hydrographic Practice

Okpuvwie Ejuvweyere Jonathan* Garba Mustapha

Department of Geographic Information Science, African Regional Institute for Geospatial Information Science and Technology (AFRIGIST), Obafemi Awolowo University Campus, Ile-Ife, Nigeria

ABSTRACT

Any seafarer or mariner that uses the sea knows that navigation without correct charts is impossible and hazardous because nautical charts are the most essential and indispensable tools for vessels to sail safely at sea. For vessels to safely sail at sea, the seas and the oceans ought to be charted and this falls within the domain of hydrography. However, the seas cannot be charted effectively in the absence of the deployment of human resources and adequate tools like satellite and aerial imagery, survey boats and other equipment that will facilitate the hydrographic operations. The acquisition of data and information about the sea depths, nature of sea bed, waterways, navigational hazards and navigational objects among others, basically falls within the sphere of hydrography which is primarily known as survey at sea. The paper offers a review of geospatial technologies in hydrographic practice for enhanced safety of navigation at sea. The review is important to both the mariners, shipping industry and the government in order to explore the potentials provided by Geographic Information System, Remote Sensing, cloud GIS, big data GIS and Global Positioning System to enhance the practice of hydrography. The data and materials used for the review were obtained from literature in the internet and other published works. The paper looked at hydrography as a profession, roles of geospatial technologies in hydrographic practice, benefits of hydrography to national development and finally, the weaknesses of geospatial technologies in hydrographic practice were equally examined.

1. Introduction

The oceans and the seas are gifts of nature which man can explore for his own advantage. Over 90 percent of the world's trade is conducted through the sea [1]. The maritime sector of any economy develops the capacity to bring about lasting development as different business opportunities abound in dredging and other aspects relating to maritime transportation among others [2]. For this to happen, mariners need to know the safest route to navigate their vessels, ships/crafts in order to arrive at their respective destinations safely without causing any form of structural damage to their vessels or grounding. The safe

*Corresponding Author:
Okpuvwie Ejuvweyere Jonathan,
Department of Geographic Information Science, African Regional Institute for Geospatial Information Science and Technology (AFRIGIST), Obafemi Awolowo University Campus, Ile-Ife, Nigeria;
Email: okpuvwie37@yahoo.com

navigation of ships from one point to another across the seas/oceans falls with the domain of hydrography which is solely responsible for the production of charts and other nautical publications for safe navigation.

Hydrography is an applied discipline that deals with the systematic observations of the sea and all its characteristics as it affects the safe navigation of ships from one point to another. Hydrography also deals with the taking of measurement of various features of the water bodies. The profession gathers different types of information relating to the depth and height of the sea as well as tide and tidal information among others. This applied profession is the master key that is used for proper management of the seas and waterways.

Hydrography according to the International Hydrographic Organization (IHO) "is a part of the discipline of applied science that relates with the taking of relevant measurements at sea and description of various features of the water bodies for the sole aim of navigation and all other marine purposes and activities, including – inter alia- offshore activities, research, protection of the environment, and prediction services" [3]. Hydrography encompasses different activities such as measurement and exploration of various features of water bodies [4]. For the safe navigation of ships and vessels or crafts at sea, mariners need to know which aspect of the sea is deep, shallow, safe and navigable in order to enable their vessels safely arrive at their respective destinations. This is where hydrography comes in. The hydrographer who is a specialist in the field of hydrography, vast in maritime-related affairs has several options as well as methods at his disposal to ensure that the information he provides to the mariners are correct and accurate for safe navigation [4].

Among the several options and methods opened to the hydrographer is the use of geospatial technologies. Geospatial technologies involve the use of Remote Sensing (RS), cloud GIS, Global Positioning System (GPS) and Geographic Information System (GIS) to collect, collate, integrate, store, manage and manipulate geographic data in order to solve geographic problems. This review is aimed at exploring the potentials of geospatial technologies in hydrographic practice for enhanced safety of vessels at sea.

2. Materials and Methods

The materials used for this review were obtained from works of various scholars in the internet and documents of both local and international hydrographic and maritime organizations and agencies. The paper adopted descriptive methodology in this work for better analysis.

3. Literature Review

3.1 Hydrography as a Profession

Hydrographic data are generally in large demand across the globe for protection, preservation and management of the marine environment [5]. Hydrography is an applied science which is basically associated with the study of the bodies of water (including surface and subsurface) and all the varying characteristics primarily aimed at ensuring the safe navigation of ships, vessels or crafts from one point to another across the seas, rivers and oceans.

All hydrographic practices are regulated across the world by the International Hydrographic Organization (IHO). The IHO was formed in 1921 and has 93 Member States. It primarily supports the coordination and setting of hydrographic ethics and creates global awareness on the usefulness of hydrography. To achieve this, 21 of June of every year has been declared by IHO to mark world hydrography day.

Hydrography is basically associated with the production of charts and other nautical publications for safe navigation. Generally, ultimate accuracy is required in the production of nautical charts [6]. The field of hydrography cut across several disciplines like physics, cartography, geodesy, geomatics, software development, mathematics, geography, surveying, data management, remote sensing, engineering, technological designs, electronics and computer applications among others [7,8].

Through hydrography, a number of nautical publications are produced to aid the mariners for safe navigation of their vessels at sea. The hydrographer performs several tasks to ensure that vessels and ships at sea navigate safely to their respective destinations. The hydrographer conducts a detail measurement and description measures of water bodies such as rivers, lakes and oceans among others. All these tasks must be conducted in a methodical, systematic and orderly manner because any data that is correctly collected will not be useful if it is not processed diligently and logically [4].

Hydrographic data are a useful asset for any activity at sea and in coastal areas. In the context of marine GIS, hydrographic data no doubt become a primary data source [9]. The hydrographic data are collected by using various state of the art gadgets. These instruments enable the hydrographer to effectively conduct his activities both at sea and on land, as some of the instruments are integrated and mounted on sea and air platforms. Some of the equipment include sounding poles, Side scan sonar, echo sounder, GPS, Survey Vessels / Survey Boats, and Software tools like Hydro CAD, HYPACK, ArcGIS among others [4]. Figures 1, 2 and 3 respectively

show some of the various hydrographic equipment and a hydrographic survey boat used at sea.
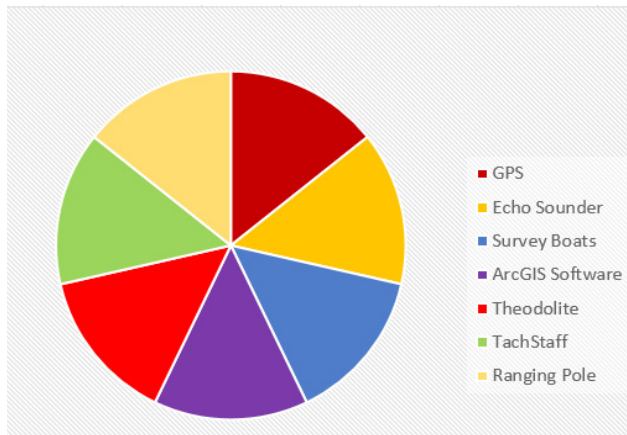

Figure 1. Some Types of Hydrographic Equipment

Source: Authors' analysis (2021)

A typical small hydrographic launch used for near-shore and harbour surveys

Figure 2. A Hydrographic Survey Boat

Source: Adapted from IHO Publication M-2 (2018)

Figure 3. A Hydrographic Survey Ships and Boats

Source: Adapted from Iptes (2014)

At the international level, the IHO accredits and recognizes some institutions that offer hydrographic education to both individuals and corporate organizations. Some of the IHO recognized hydrographic institutions include RAN Hydrographic School, Balmoral Australia, Royal Naval Hydrographic School, Plymouth UK and National Institute of Hydrography GOA, India, among others.

The training programme in hydrography are generally classified into different categories. These standards are promulgated in IHO Publication S-5 [10] and S-8 [11]. These categories define the level of competence and by extension the qualifications and the expectations required from the individual in the course of his/her hydrographic training. Thus, there are category A programmes, category B programmes and unclassified programmes and the scheme system [10,4].

The programmes in Category A provides the fundamentals. The programmes in "A" Category provides a detail knowledge in all aspects of the discipline for persons who will practice analytical reasoning and decision making. The programmes in Category "B" introduces subjects from the perspective of a practical level. Category "B" programme which is a subset of category A, provides the opportunity for learners to have a full grasp of the practical aspect of the profession. Learners who have training in Category A or B may be seen as fit and competent to be certified as Hydrographers [10,4,12]. The IHO clearly defined four orders of surveys to be conducted at sea. These are: Special Order, Order 1, Order 2 and Order 3 [11]. Table 1 shows the orders of hydrographic surveys.

It is however, instructive to note that hydrography is a dynamic profession and changes from time to time due to ocean dynamics and changes, hence the above hydrographic survey orders were however modified from four to five [13] Edition 6.0 published in 2020. The five hydrographic surveys orders include: Exclusive Order, Special Order, Order 1a, Order 1b and Order 2. The general characteristics of the five orders are holistically examined in the succeeding paragraphs.

Exclusive Order: The Exclusive Order of hydrographic surveys is an elongation of IHO Special Order. This order has more rigorous uncertainty and data reporting requirements than the order sets of hydrographic survey orders. The exclusive order is planned to be limited to shallow water areas such as harbours, berthing areas and critical areas of fairways and channels where there is an exceptional and optimal use of the water column and where specific critical areas with minimum underkeel clearance and bottom characteristics are possibly hazardous to vessels. For this order, a 200% feature examination and a 200% bathymetric

coverage are mandatory. The size of features to be spotted is deliberately more tedious, strenuous and challenging than for Special Order.

Table 1. Orders of Hydrographic Surveys

ORDER	Special Order	Order 1	Order 2	Order 3
Examples of Typical Areas	Harbours, berthing areas, and associated critical channels with minimum underkeel clearances	Harbours, harbour approach channels, recommended tracks and some coastal areas with depths up to 100 m	Areas not described in Special Order and Order 1, or areas up to 200 m water depth	Offshore areas not described in Special Order, and Orders 1 and 2
Horizontal Accuracy (95% Confidence Level)	2 m	5 m + 5% of depth	20 m + 5% of depth	150 m + 5% of depth
Depth Accuracy for Reduced Depths (95% Confidence Level)	a = 0.25 m b = 0.0075	a = 0.5 m b = 0.013	a = 1.0 m b = 0.023	Same as Order 2
100% Bottom Search	Compulsory	Required in selected areas	May be required in selected areas	Not applicable
System Detection Capability	Cubic features > 1 m	Cubic features > 2 m in depths up to 40 m; 10% of depth beyond 40 m	Same as Order 1	Not applicable
Maximum Line Spacing	Not applicable, as 100% search compulsory	3 x average depth or 25 m, whichever is greater	3-4 x average depth or 200 m, whichever is greater	4 x average depth

Source: Adapted from IHO Standards for Hydrographic Surveys, Publication S-44, 5th Edition 2008

Special Order: The Special order is envisioned for those areas where underkeel clearance is life-threatening. The precise areas that is essential for this kind of order include: berthing areas, harbours, and critical areas of fairways and shipping channels. In this order of survey, a 100% feature exploration and 100% bathymetric coverage are compulsory and the size of the features to be sensed by this search is intentionally more difficult than for Order 1a.

Order 1a: The Order 1a survey is projected for areas where features on the bottom may become a source of apprehension for the type of surface traffic anticipated to move across the area but where the underkeel clearance is seen not to be critical. Instances of areas that may need Order 1a surveys are coastal waters, harbours, berthing areas, fairways and channels. In this type of survey order the search for underwater features is 100% so as to effectively find features of a stated size. Also, bathymetric coverage less than or equal to 100% is suitable as long as the least depths over all significant features are found. The bathymetry offers acceptable representation of the kind of the bottom landscape. Underkeel clearance becomes less critical as depth increases, so the size of the feature to be spotted increases with depth in zones where the water depth is greater than 40 metres.

Order 1b: The Order 1b is envisioned for places where the kind of surface vessels projected to move across the area is such that an overall representation of the bottom is seen to be suitable. 5% bathymetric coverage is essential as the minimum for the survey area. This implies that some underwater features will not be noticed, however the distance between places of bathymetric coverage will limit the size of those features. This order of survey is only suggested where underkeel clearance is seen not to be an issue. An instance of this would be an area where the bottom characteristics are such that the probability of there being a feature on the bottom that will jeopardize the type of surface vessel anticipated to circumnavigate the area is low.

Order 2: The Order 2 hydrographic survey is considered to be the smallest strict order and is proposed for places where the depth of water is such that an overall representation of the bottom is seen as appropriate. In this order, 5% minimum bathymetric coverage is mandatory for the survey area. It is suggested that Order 2 surveys are carryout in areas which are deeper than 200 metres. Once the water depth surpasses 200 metres, the presence of features that are big enough to influence surface navigation and yet still remain unnoticed by an Order 2 survey is seen to be doubtful.

3.2 Some Donor Agencies that Fund Hydrographic Projects

There are some international organizations and agencies that fund and support hydrographic projects around the world. Some funding for hydrographic projects can be obtained from these agencies as shown in Figure 4.
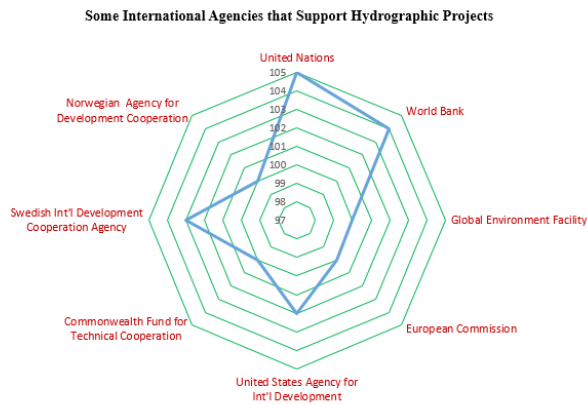
Figure 4. Some Donor Agencies for Hydrographic Projects

Source: Authors' analysis (2021)

3.3 Roles of Geospatial Technologies in Hydrographic Practice

Modern hydrographic practices have incorporated geospatial technologies in ensuring the production of accurate and reliable products. Geospatial technologies involve the use of GIS, RS, cloud GIS, big data GIS and GPS to collect, manage, integrate, store and manipulate geographically referenced data in order to provide solutions to geographic problems. [14] posited that there are some recent means to carryout mapping of coastline aerial and high-resolution satellite imagery and ground-based surveying. Just like what is obtainable in other professions, geospatial technologies serve as the pillar of hydrography. GIS is a tool and a container of maps stored in a digital format which can be used to solve geographic problems for the benefit of mankind [15]. The technology includes people, data, hardware, software and procedure(method) as components. See Figure 5.

It is imperative to note that without georeferencing or positioning, any hydrographic data will be incomplete. For the purposes of safe navigation of vessels, ships and crafts at sea, both the oceans, seas ought to be charted properly at all time. For this to be achieved, the use of satellite and aerial imagery need to be considered and this is the main domain and focus of remote sensing. Remote sensing is the scientific technique that deals with the collection of data without having any form of physical contact with the acquired data. This can be done through aircraft, satellites and drones. It is the acquisition of information relating to an object under investigation with instruments used in the acquisition of the data having no physical and direct contact with the phenomena under investigation [16]. Remote sensing uses a part or several parts of the electromagnetic spectrum during the acquisition of data

from the earth and provides the medium to observe from the space, the activities of human beings [17]. Through this method, data relating to hydrography can also be acquired, investigated, analyzed and interpreted to solve geographic problems.
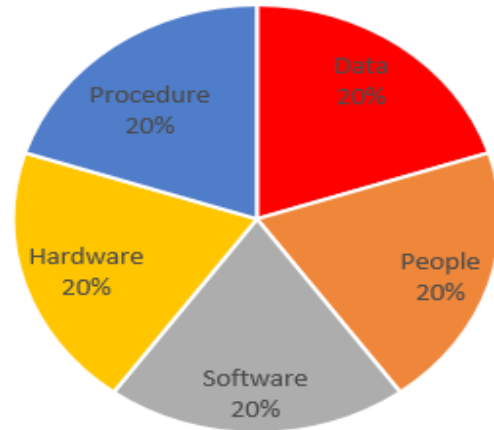
Figure 5. Components of GIS

Source: Authors' analysis (2021)

Difficult areas that are inaccessible at sea can be reached through remote sensing with the aid of aircraft and drones. The effective mapping of the oceans and the seas is necessary because, they form the resource base upon which the extraction of resources, food, medicines, transport and infrastructure rest upon [8]. In today's world, digital charts used for navigation have gradually replaced traditional nautical charts, as mariners are spared with the burden of conveying huge volume of paper charts. GIS as a modern geospatial technology has the capability of manipulating and overlaying large volume of data. With GIS, thematic layers and maps can be created and generate specific models. With GPS, coordinate points of hydrographic features of interest can be collected, stored and retrieved. The retrieved information can be interpolated and presented in a Microsoft Excel format that will later be transferred into an ArcGIS environment for further analysis, interpretation and production of various charts and maps/graphs that will aid safe navigation of vessels/ships at sea.

Geospatial technologies are very important in the collection and gathering of data and validation. One notable area of geospatial technologies in hydrographic practice is in the area of the application of Satellite Derived Bathymetry to conduct hydrographic surveys. Despite its short comings in acquiring accurate data in respect of meeting the standards required by IHO S-44 standards, the satellite derived bathymetry can still be another valuable means to carry out the planning of

surveys at sea [18]. Both cloud GIS and big data GIS are useful for spatial and analytical modelling. Satellite imagery, aerial imagery, LiDAR, GPS and drones/ unmanned aerial vehicles among others are master technologies that can actively and effectively play a crucial role in hydrographic practice [8].

3.4 Benefits of Hydrography in National Development

The development of any nation encompasses all sphere of human endeavour as the maritime sector of any nation's economy performs a critical role in the growth and advancement of most societies. For this to be achieved, vessels and ships need to move safely from one point to another without endangering the life of the crew or caused structural damage to the vessel/ships at sea or harbour. This is where hydrography comes in as the production of maritime charts is a classical illustration of a community service which is one of the known hydrographic products [19].

With hydrography, nautical charts are produced, maritime safety information and digital data are made available to the shipping industry to support and promote the needs of our maritime world. Hydrography determines the depth of the seabed, examines the various characteristics of the seabed, water, current and dangers/obstruction to safe navigation. A rich source of data for making decisions about a nation's territorial waters can be provided through the aid

of hydrographic survey and remote sensing of the marine environment. Hydrography plays an important role in both maritime and coastal development of any nation [20]. The total economic and commercial benefits of hydrography are not easy to measure. Numerous studies conducted on the benefits of hydrography have estimated that the return-on-investment for coastal nations to have, maintain, develop and provide hydrographic services is on the ratio of 1:10 due to the contribution of hydrography towards the development of blue economy (IHO, 2004; cited in [19]). This ought to be a morale booster for coastal nations to develop their hydrographic offices in order to boost their national income. Both the government and private sector require hydrographic data. Hydrography supports every activity that is connected and linked with the sea, including safety of navigation, economic development, defence, port construction and environmental protection among others [21]. See Figure 6.

The science of hydrography and oceanography help both mariners including members of the armed forces to safely navigate their vessels to their various destinations by uninterruptedly monitoring courses and steering areas as well as charting the water depth, the shape of the coastline, and potential navigational threats provided by underwater features. It is also critical in managing all key actors involved in both fishing and maritime sectors, coastal zone management, port construction and dredging among other [22]. The collection and recording

Cost versus benefit ratio of investing in hydrography is more than 1:10

Figure 6. Cost Vs Benefits Ratio of Hydrography

Source: Adapted from IHO Publication M-2, (2018)

of data to support maritime operations and trade is not a novel concept. It all began with the need for seafarers to understand how to navigate rivers and oceans safely and efficiently by understanding hazards, where they are located, and safe passages around them. Competing exploring and trading nations were sometimes denied access to vital hydrographic and charting information for economic, military, and territorial gain. This attitude changed in recent years with the establishment of national hydrographic offices around the world [23].

It is imperative to note that every activities of human that take place on the planet earth, or under the sea need a fair knowledge of the hydrography of that environment, which comprises of the nature of the seafloor, and hazards to navigation. This is because, without hydrography, vessels cannot sail effectively, construction of sea ports will be impossible, and the development of coastal infrastructures will be difficult and there will be no delimitation and enforcement of maritime boundary. The safe and efficient navigation of vessels at sea, engendering of national maritime development, safeguarding life and property at sea, supporting the protection of the marine environment and aiding the management and sustainable development of the national maritime zones are some of the areas Hydrography plays a dominant role. Hydrography is also useful to national security and maritime defense [24]. The expansion of global trade has been enhanced through hydrography in recent years. Furthermore, many coastal state governments are oblivious of the significant contribution that hydrography and nautical charting services can render to their country's economic growth [24]. Additionally, hydrography is critical in the collection of bathymetric data in the field of marine science. Bathymetry from national hydrographic services is used in local and regional models for different scientific studies such as, positioning and placement of scientific equipment and other aspects of marine science [24].

Maritime accidents are prevented through hydrographic data in different ways. First, it identifies navigational hazards and allows ships to safely avoid them. Second, they help to reduce human error in navigation, which is currently one of the leading causes of shipwrecks, by "providing data for electronic navigation (in which ships' positions from satellite are continuously displayed with chart information [25]. [26] opined that hydrography supports the blue economy. To him, the blue economy, which generates jobs and wealth for the World We Want, is built on Hydrography. He further defines hydrography as the production of nautical charts and publications, as well as the sharing of Maritime Safety Information (MSI). The IHO considered MSI as the first phase in hydrographic capacity building [27]. This MSI contains all information

relating to the safety of navigation of vessels at sea, including notices to mariners, navigational warnings, and information about the seafloor that may pose a danger to vessels. Thus, one of the primary responsibilities of hydrography is the complete search of the seafloor using side scan sonar. Figure 7 depicts a side scan sonar used to detect and image objects on the seafloor.
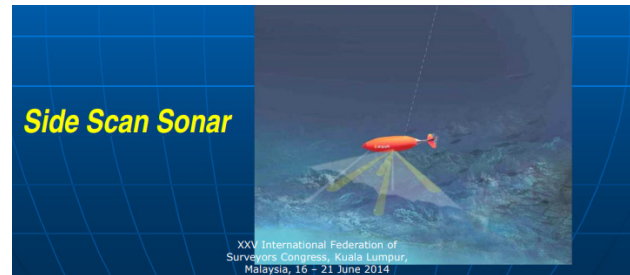
Figure 7. A Side Scan Sonar for Detecting and Imaging Objects on the Seafloor

Source: Adapted from Iptes (2014)

Hydrographic survey helps in the control and planning of engineering projects like bridges, dams and reservoirs among others. Other useful aspects of hydrography to national development are succinctly discussed in the succeeding paragraphs:

3.4.1 Maritime Transport/Navigation

The chief cornerstone and mainstay of global trade are maritime transportation. A major obstacle militating against the progress of most countries' economy, especially coastal states is the lack of a well maintained and adequate port facilities. For safe navigation of ships/ vessels/crafts at sea, the mariner needs navigational or nautical charts for direction. Nautical charts show the depth of the sea and associated dangers. This is where the profession carries out a dominant work in producing nautical charts, sailing direction, tide tables and other relevant nautical publications. Over 90 percent of the world's trade is conducted through the sea [1]. One of the major elements to consider for a nation's economy is maritime commerce.

3.4.2 Maritime Defence and Security

Maritime defence and national security are becoming a major aspect of national defence policy of most nations across the world. The role of the navies/coast guards of nations is gradually expanding on daily basis as the navies/coast guards need critical information about the territorial waters for safe navigation of their ships/vessels and amphibious crafts/boats. For successful amphibious

assaults to be conducted by the navy/coastguards against all sorts of maritime criminals, the navy needs vital hydrographic information relating to the depth of the assaulted area, and an in-depth knowledge of tidal information in planning for marine based operations [28].

The navies/coast guards are major users of nautical charts produced by hydrographic offices around the world. The navies/coast guards must be ready at all time for deployment of both human and material resources to different parts of the world either for peace keeping or assault operations, hence they need to maintain a sizable number of charts. The maritime data and information provided by hydrography, aid a variety of products used in naval warfare [3].

3.4.3 Coastal Zone Management

Coastal nations need the effective management of their coastal areas; hence, the government needs the input of hydrography. Relevant hydrographic information is needed for effective coastal management. Bathymetric charts and nautical charts among others are very necessary for an effective and efficient coastal zone management including flood control and erosion management [4].

3.4.4 Maritime Boundary Delimitation and Delineation

Hydrography also plays a dominant role in maritime boundary delimitation and delineation of territorial sea baseline around the world. Maritime boundaries require technical skills and are necessary for good international relations among countries [28]. Nautical charts and other products associated with hydrography are useful for different activities, including delineation and demarcation of boundaries. Charts are important in the graphical representation of maritime zones [29], and this is where hydrography comes into play as the production of nautical charts falls within the domain of hydrography.

3.4.5 National Marine Spatial Data Infrastructures

Spatial Data Infrastructures (SDI) provides the basis for arranging geographic data, metadata, tools and users with clear set out guidelines and rules, relationships and standards. Marine SDI is not meant to be disconnected from other SDIs but plays a complementary role in the coastal zone and oceans [9]. Many nations around the world establish national spatial data infrastructures because they believed that good quality spatial data are key to economic growth and prosperity. SDI integrate various data sets such as bathymetry, topography and geodesy among others of major national spatial data providers thereby enhancing nations' national and economic development [3,4]. For effective national marine spatial data infrastructures, hydrographic data are necessary. Within the context of a marine spatial data infrastructure for wider use, hydrographic data acts as the basis for building a maritime data management system [9]. Figure 8 shows the summary of the benefits of hydrography as a profession.

There are various stakeholder ministries that collaborate with the development of hydrography across the world according to [24]. These stakeholders are very important to hydrographic practice. See Figure 9 for the different stakeholders that contribute to the growth, advancement and development of hydrography around the world.
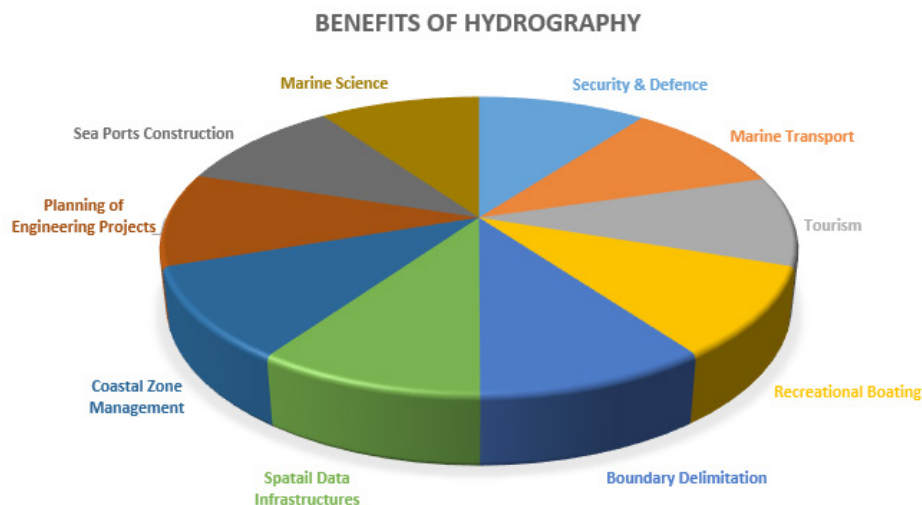

Figure 8. Benefits of Hydrography
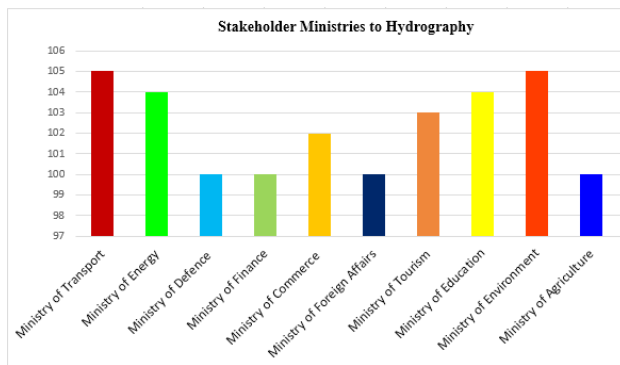
Source: Authors' analysis (2021)

Figure 9. Stakeholder Ministries to Hydrography

Source: Authors' analysis (2021)

4. The Weaknesses of Geospatial Technologies in Hydrographic Practice

Despite the strength of geospatial technologies, there are some weaknesses that are associated with these technologies. Acquired remote sensing data are expensive and the technology itself is equally expensive to come by. The effective analysis of remote sensing data and images needs a kind of specialized skills. Extra training and skills are needed by the users of the technology to be able to effectively interpret imagery. Also, the cost of acquiring aircraft, drones and UAVs is high to come by and the maintenance of the various parts and accessories is always difficult and tedious. Extreme weather conditions can also affect the effective deployment and use of aircraft, drones and UAVs, hence the need to properly liaise with before
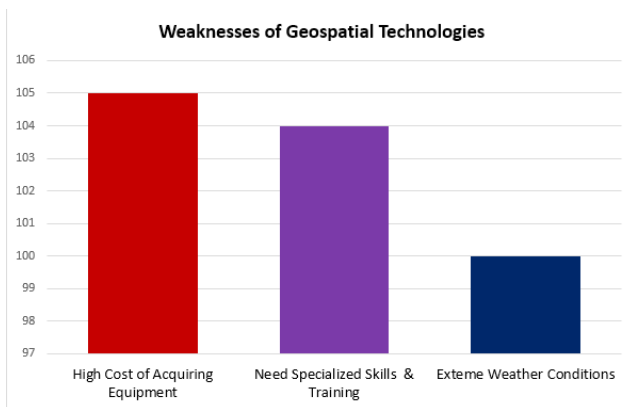

Figure 10. Weaknesses of Geospatial Technologies in Hydrographic Practice

Source: Authors' analysis (2021)metrological stations

embarking on the use of these devices. The failure to adhere to weather conditions can lead to blurred data and images which will invariably affect the quality of the end products. GIS also has its own weaknesses, for instance,

GIS technology requires trained and skillful experts that need to interpret, analyze and interpolate all collected data. Besides, GIS software are expensive to acquire and this could hinder effective data gathering, analysis and interpretation. The summary of the weaknesses of geospatial technologies in hydrographic practice is shown in Figure 10.

5. Conclusions

The roles of hydrography in national development cannot be overemphasized. With the aid of hydrography, nautical charts and other nautical publications that are required by the mariners to safely navigate their ships/ vessels from one point to another across the vast seas and oceans of the world are produced. Hydrography and geospatial technologies are twins and inseparable as they help in fostering safe navigation at sea. With hydrography, coastal nations can develop and maintain their coastal zones, improve on their marine transport and maintain marine spatial data infrastructures among others. Having critically and holistically reviewed hydrographic practice and geospatial technologies, the paper therefore recommends that coastal nations around the world should integrate and incorporate geospatial technologies into their hydrographic practices for enhanced navigational safety of vessels/ships at sea.

References

[1] Laryea, D., 2019. 90 Percent of World Trade is By Sea-Official, APA News. Regional Coordinator of the International Maritime Organization for West and Central Sub-Region of Africa.

[2] Jamoh, B., 2020. Maritime Security and National Development in Nigeria: The Role of NIMASA. A Paper Delivered by the Director-General of NIMASA, Dr Bashir Jamoh at the National Defence College for Course 29 participants, Abuja, Nigeria.

[3] Anonymous, 2005. Manual on Hydrography, Publication C-13. Published by the International Hydrographic Bureau, Monaco. First Edition.

[4] Udoh, I., Eyoefen, I., 2013. A Career in Hydrography: The Intricacies and its Make-Up. A Paper Presented at the FIG Working Week 2013, Abuja, Nigeria. Theme: Environment for Sustainability.

[5] Anonymous, November 2020. IHO-International Hydrographic Organization Strategic Plan for 2021-2026.

[6] Verstelle, J.T., 18 January 2010. Hydrographic Surveying-Admiralty Manual of Hydrographic Surveying, Vol. 1. XIV, Published online by Cambridge

University Press.
DOI: https://doi.org/10.1017/s0373463300047688

[7] Sangeeta, D., 2016. How GIS Helps Drive Hydrography Data. GIS Lounge.

[8] Ponce, R., 2014. The New Role of Hydrography in the 21st Century: Evolving from Charts to Geospatial Data. Hydro International.

[9] IHO-International Hydrographic Organization, May 2011. Standards of Competence for Hydrographic Surveyors,'' Publications S-5, 11th Edition, Version 10.0.1,Accessed 2 August 2021. http://www.iho/int/ iho pubs/standard/ S-5 Ed 10.0.1 06may2011 standards-Hydro.pdf.

[10] Anonymous, April 1998. IHO-International Hydrographic Organization Standards for Hydrographic Surveys 4th Edition, Special Publication No. 44.

[11] Furness, R., 2021. Education in Hydrographic Surveying and Nautical Cartography. The International Board on Standards of Competence for Hydrographic Surveyors and Nautical Cartographers, International Hydrographic Review. No 25.

[12] Anonymous, September 2020. IHO-International Hydrographic Organization Standards for Hydrographic Surveys. S-44 Edition 6.0.0.

[13] Fadahunsi, O., Pe'eri, S., Armstrong, A., 2014. Characterisation of the Nigerian Shoreline: Making Use of Publicly Available Satellite Imagery. Hydro International.

[14] Somvanshi, S., 2021. Implementation of GIS Technology in Modern Development. A Lecture Organized by TEAM 2020 HELPERS (Non-Profit Organization- West Bengal, India) in Association with UNIQUE MAPPERS TEAM, Nigeria.

[15] European Space Agency, 2016. What is Remote Sensing? Available:http://www.esa.int/SPECIALS/ Eduspace_EN/SEMF9R3Z2OF_0.html (Accessed 28 July 2021).

[16] Levin, N., Christopher, C.M.K., Qingling, Z., Alejandro, S., Miguel, O.R., Xi Li, B.A.P., Andrew, L.M., Andreas, J., Steven, D.M., Zhuosen, W., Ranjay, M.S., Christopher, D.E., 2020. Remote Sensing of Night Lights: A Review and an Outlook for the Future. Remote Sensing of Environment. 237.
DOI: https://doi.org/10.1016/j.rse.2019.111443

[17] Pe'eri, S., Azuike, C., Parrish, C., 2013. Satellite-Derived Bathymetry: A Reconnaissance Tool for Hydrography. Hydro International.

[18] Connon, B.D., Nairn, R., April 2010. Economic Benefits of Hydrography. FIG Congress 2010, Facing the Challenges – Building the Capacity, Sydney, Australia. 11-16.

[19] Soenhadi, B.A., 2016. International Seminar and Workshop on Hydrography: Roles of Hydrography in Marine Industry and Resources Management. Being an International Seminar Held in Indonesia.

[20] Niazi, M.A.K., 2021. A Message from the Pakistan Chief of the Naval Staff on the Occasion of World Hydrography Day.

[21] Ojinnaka, O.C., May 2013. Hydrography in Nigeria and Research Challenges. TS05E - Hydrographic Education and Standards – 6439, FIG Working Week 2013, Environment for Sustainability Abuja, Nigeria. 6-10.

[22] Petrica, P., Emanuela, M., Lucian, D., 2021. A New Approach to the Development of Hydrography. Hal 20 Archives Ouvertes, https://hal.archives-ouvertes. fr/hal-03334182.

[23] Ward, R., Bjørn-Andersen, N., 2021. The Origins of Maritime Informatics. In: Lind M., Michaelides M., Ward R., T. Watson R. (eds) Maritime Informatics. Progress in IS. Springer, Cham.
DOI: https://doi.org/10.1007/978-3-030-50892-0_1

[24] International Hydrographic Organization, 2018. The Need for National Hydrographic Service, IHO Publication M-2, Version 3.0.7.

[25] Nairn, R., 2010. The Challenge of Hydrographic Surveying and Charting the Antarctic. TS 91 – Nautical Charting – Marine Cartography.

[26] Iptes, M., 2014. Hydrography, Nautical Charts, Marine Spatial Data Infrastructure and Blue Economy for the "World We Want." XXV International Federal.

[27] International Hydrographic Organization, 2017. IHO Capacity Building Programme. The State of Hydrography and Nautical Charting in Republic of Azerbaijan.

[28] Beckman, R., Bundy, R., Carleton, C., Davenport, T., Pratt, M., 2011. Maritime Boundary Delimitation. A Training Workshop Programme 2011, Organized by Centre for International Law and the Faculty of Law, National University of Singapore.

[29] Kastrisios, C., Tsoulos, L., 2017. Maritime Zones Delimitation – Problems and Solutions''. Proceedings of the International Cartographic Association. 1.
DOI: https://doi.org/10.5194/ica-proc-1-59-2017, 2020.

ARTICLE

Agarase Production by Marine *Pseudoalteromonas* sp. MHS: Optimization, and Purification

Mona M. Sharabash[1]   **Samia S. Abouelkheir**[2*] ⓘD   **Mona E. M. Mabrouk**[3]   **Hanan A. Ghozlan**[1]
Soraya A. Sabry[1]

1. Botany and Microbiology Department, Faculty of Science, Alexandria University, Alexandria, 21321, Egypt
2. National Institute of Oceanography and Fisheries (NIOF), Marine Environment Division, Marine Microbiology Laboratory, Egypt
3. Botany and Microbiology Department, Faculty of Science, Damanhour University, Damanhour, Egypt

ARTICLE INFO	ABSTRACT

Agar is an essential polysaccharide that has been utilized in numerous fields. Many kinds of literature have been published regarding agarolytic microorganisms' isolation and agarases biochemical studies. In this search, a local marine agarolytic bacterium associated with marine alga *Ulva lactuca* surface was isolated and identified as *Pseudoalteromonas* sp. MHS. The agarase production was parallel to the growth of *Pseudoalteromonas* sp. MHS as cells displayed a lag phase (2 h), subsequently an exponential growth that prolonged till 10 h where maximum growth (OD550nm = 3.9) was achieved. The enzyme activity increased rapidly as cells increased exponentially where the maximum activity of 0.22 U/mL was achieved after 8h and remained constant till 12 h during the stationary phase of growth. Agarase production was optimized using Plackett-Burman statistical design by measuring enzyme activity as a response and the design was validated using a verification experiment; the activity of the enzyme increased from 0.22 U/mL to 0.29 U/mL. *Pseudoalteromonas* sp. MHS agarase was partially purified and its molecular weight (MW) was determined by SDS-PAGE (15-25 kDa). Agarase showed approximately 94% of its activity at 40 °C. The enzyme stability decreased as the temperature increased; the enzyme could retain about 98, 90, 80, 75, and 60% of its activity at 20, 30, 40, 50, and 60 °C, respectively. Biomass of the red alga *Pterocladia capillacea* proved to be a suitable substrate for agarase production using *Pseudoalteromonas* sp. MHS; the enzyme activity recorded after 24 h of incubation was 0.35 U/mL compared to 0.29 U/mL from the optimized medium.

*Corresponding Author:
Samia S. Abouelkheir,
National Institute of Oceanography and Fisheries (NIOF), Marine Environment Division, Marine Microbiology Laboratory, Egypt;
Email: samiaabouelkhir@yahoo.com

1. Introduction

Agarases are hydrolytic enzymes found in a wide variety of marine organisms. They're used in biotechnological and commercial operations like decomposing algal polysaccharides, liquefaction of agar and agarose gels, biofilm removal in bioreactors, and the creation of simple sugars, along with in the food sector to make bread, beverages, and low-calorie foods [1]. The major component in the cell wall of red algae is agar, which is made up of agaropectin and agarose. To make this complex polysaccharide available for microorganisms, agarases which can hydrolyze agar into oligosaccharides or monosaccharides are necessary [2]. Many important qualities of oligosaccharides generated from agar include delayed starch degradation, bacterial growth suppression, anticancer and antioxidant actions, etc. [3].

Macroalgae are important primary producers in coastal environments, accounting for a large portion of the biomass and having an ecological role [4]. The study of the epiphytic microbiota of algae remains unexplored despite their huge biodiversity. Furthermore, because these microorganisms interact with algae, they're thought to be a good source of algal-specific enzymes (e.g., carrageenases, agarases, and alginate lyases) [5,6].

Ulva represents a vital structural constituent of coastal intertidal environments and acts as a microbial community's starting point. These communities attached to living surfaces, especially those associated with marine macroalgae of the genus *Ulva*, are recognized to harbour a large number of accompanying microorganisms with host-specific colonisation configurations that are influenced by macroalgae features such as cell wall constituents and defence mechanisms [7]. The creation of these polysaccharides by macroalgae encourages epiphytic bacteria to produce enzymes that can breakdown a wide range of compounds [5]. Comba-González et al., (2016) [1] constructed a flowchart illustrating the various investigational procedures intended for recognizing enzymes generated by *Ulva* associated-epiphytic bacteria.

Many bacteria have been found in saltwater and marine sediments that can hydrolyze and metabolise agar as a carbon and energy source, creating agarases, which catalyse the hydrolysis of agar [8]. Agarolytic bacteria are classified into two classes based on their ability to digest
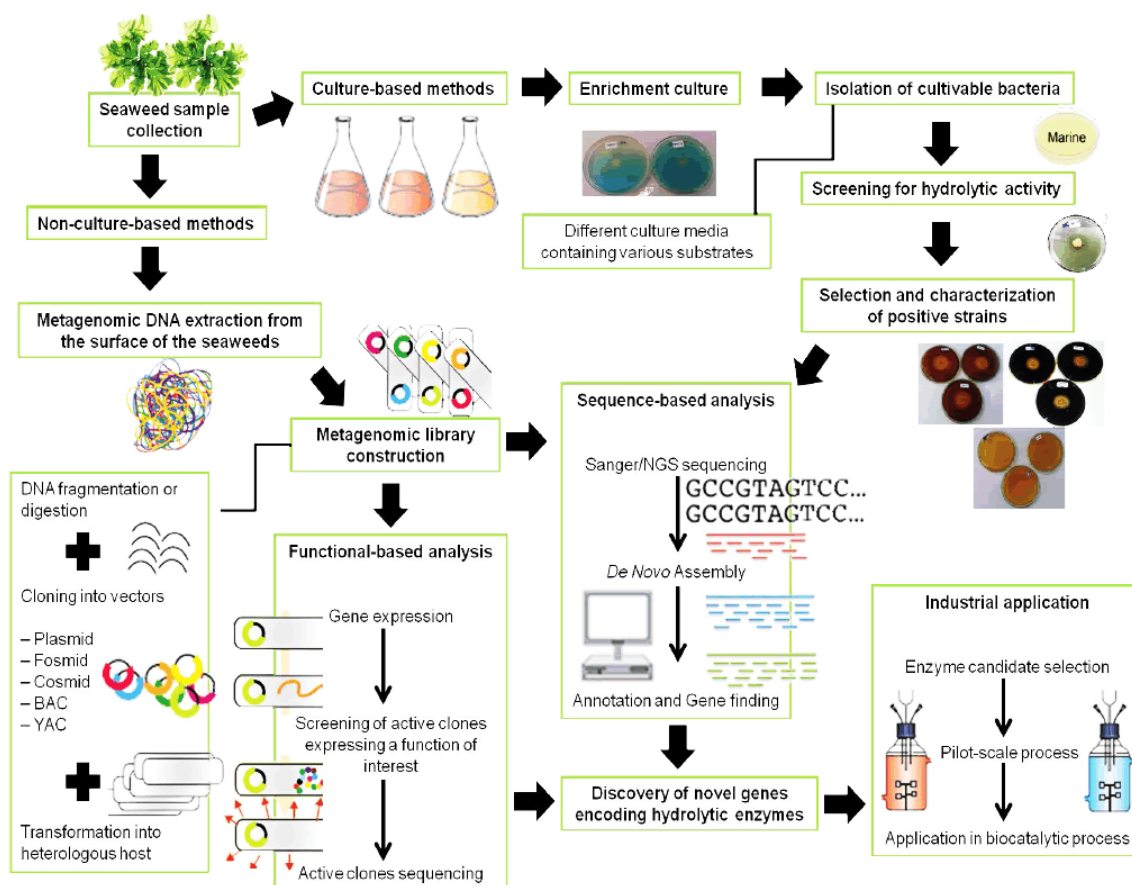

Figure 1. A schematic representation depicting the various experimental approaches used to study macroalgal epiphytic bacteria and their hydrolytic enzymes [1].

solid agar. Bacteria in group I soften the agar, causing depressions adjacent to the colonies, while bacteria in group II cause the agar to liquefy extensively [9]. Because agar is a polysaccharide generated by marine seaweeds, most agarolytic bacteria originally obtained from marine habitats; they include *Pseudomonas* sp. [10], *Pseudoalteromonas* sp. [11], and *Micrococcus* [12]. Only a few strains, such as *Streptomyces coelicolor* A3 (2) [13] and *Streptomyces lavendulae* UN-8 [14], have been identified from non-marine environments. *Pseudoalteromonas* species are commonly detected in the presence of marine eukaryotes [15,16]. *Pseudoalteromonas* species have been found to produce a number of enzymes that aid in the degradation of polysaccharides derived from marine algae such as alginate, agar, and carrageenan [11].

Up to our knowledge, there are just a limited numbers of publications linked to the improvement of agarase production using wild type bacteria that we are aware of [17-19]. Statistical designs have thus been successfully employed to improve the productivity of several bioprocesses [18]. The Plackett-Burman design (PB) cuts down on the number of tests while still producing relevant findings. The first stage is to use a fractional factorial design to assess the comparative significance of numerous ingredients within a complex culture media, selecting levels of variables that have substantial effects on enzyme activity. The optimal medium's validity is checked against the basal medium and anti-optimum one as a second step. If n factors are to be explored in this study, a complete factorial design would necessitate 2^n experiments [18].

Therefore, the target of the current search was to isolate and identify a marine agarolytic bacterium from the epiphytic microbiome of the green macroalga *Ulva lactuca*. It is also aimed to elucidate the factors affecting agarase production employing Plackett-Burman experimental design. In addition, partial purification of the enzyme was considered. Furthermore, biomass of the red seaweed *Pterocladia capillacea* was evaluated as a substrate for agarase production using *Pseudoalteromonas* sp. MHS.

2. Materials & Methods

2.1 Bacterial Strain

Pseudoalteromonas sp. MHS utilized throughout the study was isolated from *Ulva lactuca* surface collected from the Mediterranean Sea at El-Anfoushi district, Alexandria, Egypt, and identified using the 16S rRNA sequence analysis.

2.2 Microbiological Medium

The medium used in this study was nutrient broth (NB) (5 g peptone, 3 g yeast extract) dissolved in 1 L seawater and supplemented with 0.1% agar. In case of solid medium nutrient agar (NA), 1.5% agar was used for solidification and sterilized using autoclave at 121 °C for 20 min. Initial pH was 7.5.

2.3 Reagents for Reducing Sugar Estimation

Dinitrosalicylic acid (DNS) reagent: 0.2 g phenol and 0.05 g sodium sulfite were dissolved in 100 mL 1% NaOH, and 1 g dinitrosalicylic acid was freshly added to the solution just before use [20]. Rochelle salt solution: 40 g of $KNaC_4H_4O_6 \cdot 4H_2O$ were dissolved in 100 mL distilled H_2O. Lugol's Iodine Solution: Lugol's Iodine solution was prepared by dissolving 1 g iodine crystals and 2 g KI in 300 mL distilled H_2O [21]. Phosphate Buffer Saline (PBS): 20 mM PBS was prepared by dissolving 16 g of NaCl, 0.4 g of KCl, 2.88 g of Na_2HPO_4, and 0.48 g of KH_2PO_4 in distilled water to reach 1000 mL final volume at pH 7.6.

2.4 Solutions for SDS-Polyacrylamide Gel Electrophoresis

Solutions and buffers for SDS-Polyacrylamide gel electrophoresis were prepared according to A Guide to Polyacrylamide Gel Electrophoresis and Detection [22].

2.5 Sample Collection

The green alga *Ulva lactuca* was collected from the Mediterranean Sea at El-Anfoushi district, Alexandria, Egypt. The red alga *Pterocladia capillacea* was collected from Abu Qir district, Alexandria, Egypt.

2.6 Isolation of Agarolytic Bacteria

The algal thallus *Ulva lactuca* was gently washed and dispensed in a 100 mL Erlenmeyer's flask containing 20 mL sterile seawater and shacked at 150 rpm for 1h to detach the bacteria on the surface. Subsequently, 0.2 mL aliquot from flask was plated on NA medium. Agarolytic activity was determined by agar liquefaction or shallow depressions forming around the colonies after 48 hours of incubation at 25 °C. One isolate designated as MHS showing clearance zone and softening of agar around the colonies was chosen for further investigations. To confirm agarolytic activities, NA plates were inoculated with MHS and incubated at 25 °C for 2 days before being stained with Lugol's iodine solution to detect the existence of a clear zone around the colonies [23-26].

2.7 Identification and Characterization of the Selected Isolate

2.7.1 Phenotypic Characterization

Negative Stain, Capsule Stain, and KOH tests were performed according to Moyes et al., (2009) [27], Duguid,

(1951) [28], and Buck, (1982) [29], respectively. Screening for polyhydroxyalkanoate (PHA) accumulation was done by two methods; Plate assay method and slide staining method according to Phanse et al., (2011) [30].

2.7.2 Genotypic Characterization

Genomic DNA was extracted from the pure selected isolate and then analysed by electrophoresis according to the method described by Sambrook et al., (1989) [31]. The 16S *rRNA* gene was amplified by polymerase chain reaction (PCR) using the primer pair 8F:5'-AGAGTTTGATCCTGGCTCAG-3'1525R: 5′-AAGGAGGTGWTCCARCC-3′. The PCR reaction and product was sequenced using the sequencing facility provided by the U.S.B. American Company via SIGMA-Egypt.

2.8 Factors Affecting Growth of *Pseudoalteromonas* sp. MHS

The effect of temperature was examined by inoculating NB flasks adjusted at pH 7.5 with *Pseudoalteromonas* sp. MHS from previously prepared seed culture (OD$_{550nm}$≈1± 0.1) and incubated at diverse temperatures (5, 10, 15, 20, 25, 30 and 37 °C). The cultures were checked for growth after 24 h. Similarly, NB flasks were prepared with different seawater concentrations (0, 25, 75, and 100%); the pH was adjusted at 7.5 and incubated with the same condition to study the seawater requirement.

2.9 Agarase Production in Relation to Bacterial Growth

A standard inoculum (2%) from previously prepared seed culture (OD$_{550nm}$≈1± 0.1) was used to inoculate flasks each containing 20 mL of NB medium supplemented with 0.1% agar and adjusted at pH 7.5. Flasks were incubated at 120 rpm and 25 °C on a rotary shaker incubator (Scilogex SK-O330-Pro, USA). Bacterial growth and enzyme activity were evaluated at time intervals. Bacterial growth was expressed as OD 550 nm using a spectrophotometer (Optima SP-300, Japan).

2.10 Crude Enzyme Preparation, Semi Quantitative and Quantitative Activity Assay

The crude enzyme was obtained by centrifugation of bacterial culture at 10,000 x g for 10 min in microfuge (Hettich® MIKRO 120, Germany). The culture filtrate obtained after cell removal was considered the crude enzyme. A semi-quantitative assay was used to screen for agarase activity, based on the size of clearance zone of the cell free supernatant of *Pseudoalteromonas* sp. MHS. The experiment was carried out in a medium containing

only seawater amended with 15 g/L agar. The wells on agar plates were filled with 10 µl of cell-free supernatant, and the plates were incubated for 4 hours at 30 degrees Celsius. The formation of clear zones was confirmed by the addition of iodine solution. A pale-yellow zone around colonies was detected against a brown-violet background, indicating agar deterioration [23,32]. The increase in the concentration of reducing sugars was determined spectrophotometrically using the 3, 5-dinitrosalicylic acid (DNS) technique to determine agarase activity [33]. Under the assay conditions, one unit (U) of agarase is defined as the quantity of enzyme that produces 1 µmol of galactose per minute [34]. Galactose was employed as a reference reducing sugar for preparing a calibration curve.

2.11 Optimizing Culture Conditions for Agarase Production Using Plackett- Burman Design

Enhancement of some physical and nutritional factors influencing agarase production was performed using Plackett-Burman experimental design. This fractional factorial design [35] was used in this research to reflect the relative significance of several variables on agarase production by *Pseudoalteromonas* sp. MHS. In this study, seven independent variables were screened in nine different combinations according to the PB design matrix's eight runs. The selected variables included yeast, peptone, agar, pH, agitation, inoculum size, and seawater concentration. A high (+) and low (–) level was evaluated for each variable. The response was estimated using agarase activity. The following equation was used to find the main effect of each variable:

$$Exi = (\Sigma pi+ - \Sigma pi-)/N$$

Where Exi is the variable main effect, $\Sigma pi+$ and $\Sigma pi-$ are responses in trials where the independent variable (Xi) was present in high and low concentrations, respectively, and N is the number of trials divided by two. Accordingly, a main effect chart with a positive and negative signs show that the high and low concentrations, respectively, of this variable was closer to optimum. The factor that had no effect would give a value of zero if no interactions existed. To determine the variable significance, statistical t-values for equal unpaired samples were calculated using Microsoft Excel.

2.12 Partial Purification of *Pseudoalteromonas* sp. MHS Agarase Enzyme

400 mL of a 12 h old culture grown under optimized conditions were centrifuged at 10,000 x g for 10 min in a cooling centrifuge (HERMLE Z 36 HK, Germany) at 4 °C to remove the bacterial cells. The enzyme in the

supernatant was precipitated by adding 75 % saturation solid ammonium sulphate and stirring slowly for 1 hour. At 4 degrees Celsius, the solution was left overnight. Centrifugation at 12,000 x g for 15 minutes in a cooling centrifuge at 4 °C pelleted the precipitated protein that resuspended in 20 mL PBS and dialyzed against the same buffer in a dialysis bag in a refrigerator with intermittent change of buffer every 4 h for 1 day. The dialyzed sample was considered as partially purified agarase [11].

2.13 Sodium Dodecyl Sulfate-polyacrylamide Gel Electrophoresis (SDS-PAGE) of Protein

The SDS-Polyacrylamide gel electrophoresis of protein was performed according to Sambrook et al., (1989) [31]. The broad range molecular weight markers "Promega" consisting of nine clearly identifiable bands (10, 15, 25, 35, 50, 75, 100, 150, and 225 kDa) were used in the molecular weight determination of the protein.

2.14 Influence of Temperature on the Activity and Stability of the Partially Purified Agarase

The optimum temperature for the activity of the purified agarase was determined in PBS at different temperatures from 20 °C to 60 °C under the assay conditions. In this experiment, the partially purified agarase was mixed with substrate and incubated at several temperatures. The DNS method was used to determine agarase activity. The thermostability of agarase was determined via measuring the enzyme's residual activity after a 30-minute pre-incubation period at temperatures ranging from 20 to 60 degrees Celsius [36,37].

2.15 Agarase Production Using Red Seaweed Biomass by *Pseudoalteromonas* sp. MHS

The red seaweed *Pterocladia capillacea* was collected from the Mediterranean Sea at Abu Qir, Alexandria, Egypt, dried at 60 °C overnight, and ground using a porcelain mortar and pestle. A 500 μm sieve was used to attain particle size homogeneity in the final samples. 800 μl of the seed culture were inoculated in 20 mL Erlenmeyer flasks containing sterile seawater supplemented with different concentrations of the red seaweed (5, 10, 15, 20 g/L), adjusted at pH 9, and incubated at 25 °C under shaking condition (230 rpm). The agarase activity was measured for each flask at 12 and 24 h.

2.16 Statistical Data Analysis

All investigations were done in duplicates. The results were statistically analysed and accomplished by using Microsoft Excel. The data were expressed by means ± SE and ± SD. The significant values were determined at P-value < 0.05.

3. Results & Discussion

An attempt was carried out to isolate and identify of a local marine agarolytic bacteria associated with the surface of the green alga *Ulva lactuca*. Isolate MHS recovered on a nutrient agar plate (Figure 2a) showed clear zone and softening of the agar around the colonies (Figure 2b) after 2 days of incubation at 25 °C. Flooding the plates with Iodine caused the presence of pale-yellow zones around colonies in contrast to a brown-violet background (Figure 2c), which was considered a confirmation of agar-degrading activity [23,9,24].

Figure 2. MHS white mucoid colonies on NA plates after 48 h of incubation at 25 °C (a); Clear zone formation and depression around the colony (b); Yellow zone against brown background formed after flooding with Lugol's iodine solution (c).

MHS cells appeared as rods under the microscope when stained by the negative stain, and appeared to be encapsulated when stained by the capsule stain (Figure 3a, 3b). The dark blue colour of colonies after flooding the plate with Sudan Black B was taken as positive for accumulation of PHA as a storage material [30] and was further confirmed by Sudan black staining of cells as dark blue spots appeared inside red cells (Figure 3c). KOH test was used as an alternative to Gram stain; a positive result indicated that the isolate is Gram negative.
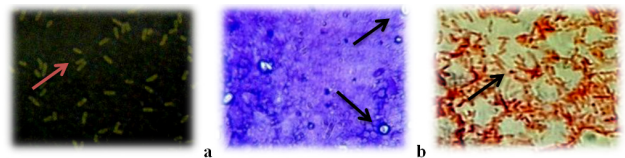
Figure 3. Light micrograph of MHS: Negative stain showing rod shape cells (red arrow) (a); Capsule stain, black arrows: colourless bacterial capsules with stained cells against dark background, Magnification×1,000. Micrograph of MHS showing the PHA granules produced in the form of dark granules in the bacterial cells (c)

Many bacterial taxa having agarolytic activity have been discovered, primarily in saltwater and marine sediment [38,25] and many reports have been made regarding

isolating agarolytic bacteria from seaweeds [39,40,34]. In a previous study, Furusawa et al. (2017) [26] stated the isolation of the agarolytic bacterium *Persicobacter* sp. CCBQB2 from *Ulva* sp. collected from a Malaysian coastal location.

In a sequential step, it was necessary to identify isolate MHS by amplifying the gene coding for the 16S rRNA using the specific primer pair mentioned in the materials and method section. The amplified fragments (1500 bps) were sequenced by the U.S.B. American Company's sequencing laboratory, SIGMA-Egypt. 16S rRNA gene sequence of MHS displayed 99% resemblance to several sequences of *Pseudoalteromonas* spp. The 16S rRNA gene sequence was deposited as KT275859 in GenBank and classified as a member of the genus *Pseudoalteromonas*, family Pseudoalteromonadaceae, order Alteromonadales, class, γ-Proteobacteria, phylum Proteobacteria and was designated as *Pseudoalteromonas* sp. MHS. The phylogenetic bond of the amplified 16S rRNA sequence and its nearby relatives was analysed using the services provided by the Ribosomal Database Project (phylogenyfr. com) and the results are summarized in the dendrogram in Figure 4.
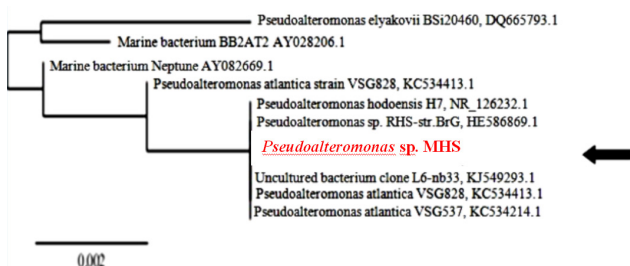

Figure 4. Shows the position of strain MHS among other closely related *Pseudoalteromonas* species in a neighbor-joining phylogenetic dendrogram based on 16S rRNA

Pseudoalteromonas (*P.*) was previously isolated from the green alga *Ulva*; Egan *et al.* (2001) [41] isolated two strains, *Pseudoalteromonas ulvae* UL12T and UL13 from the surface of *U. lactuca*, collected from the rocky intertidal zone near Sydney, on the east coast of Australia. *P. prydzensis* alex and *P.* sp. alex were also isolated from Mediterranean saltwater rocks and sponge in Alexandria, Egypt [15,16]. In addition, the agar-hydrolysing bacterium *P. hodoensis* H7 was isolated from a coastal seawater sample obtained from Ho Island in the West Sea, South Korea [11].

Pseudoalteromonas sp. MHS could grow at temperature range 5-30 °C with maximal cell growth at 30 ºC while no growth was noticed at 37 °C (Figure 5a). This indicates that *Pseudoalteromonas* sp. MHS favours the lower temperature than the higher one. Similar to the other agarase producing marine bacterium [19,11], the strain is considered a psychrotroph. Sodium chloride was

also required for MHS growth. It grew well at different concentrations of seawater but not in the absence of seawater (Figure 5b). The obtained data refer to the halophilism of the isolate and its classification as a marine bacterium.
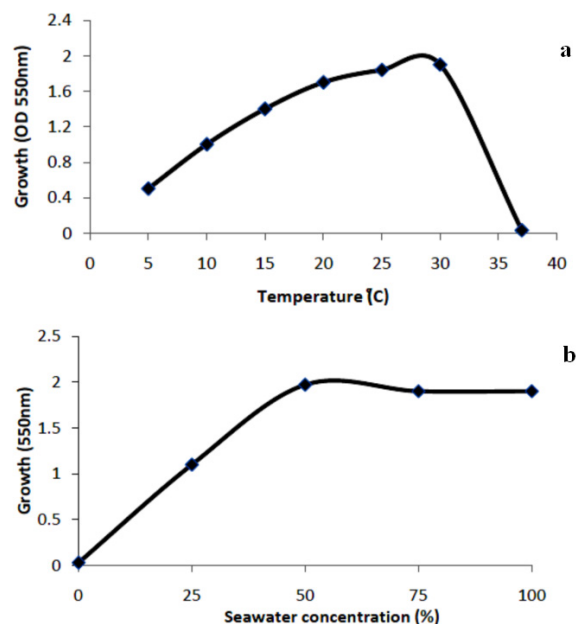
Figure 5. Growth of MHS on NB for 24 h at different temperatures (a), and with different concentrations of seawater at 25 °C (b)

3.1 Agarase Activity in Relation to Growth

Agar degradation in relation to bacterial cell growth was studied during batch fermentation in NB supplemented with 0.1% agar under shaken condition at 25 °C. Figure 6 clarifies that growth and enzyme production were parallel. Cells demonstrated a lag phase of 2 h, after that an exponential growth which prolonged till 10h where maximum growth (OD$_{550nm}$ = 3.9) was achieved. The enzyme activity increased rapidly as cells increased exponentially where maximum activity of 0.22 U/mL was achieved after 8h and remained constant till 12h during the stationary phase of growth. Based on semi quantitative assay i.e. measurement of inhibition zones formed, a zone of 16 mm was recorded just after inoculation with seed culture, and increased rapidly from 18 to 20 mm at 4-6 h reaching a maximum clearance zone of 21 mm after 8h of incubation then remained constant till 12 h of incubation (Figure 6a, 6b). The data obtained is in agreement with the previous work of Faturrahman et al. (2011) [23], and Chi et al. (2014) [11].

Figure 6. Growth and agarase activity of *Pseudoalteromonas* sp. MHS incubated at 25 °C and 120 rpm at different time intervals (a), Clearance zones resulting from the inoculation of 10 μl of cell-free supernatant of *P.* sp. MHS on agar plate (15 g/L agar in SW) and incubated at 30 °C for 4 h followed by flooding the plate with Lugol's iodine solution (b).
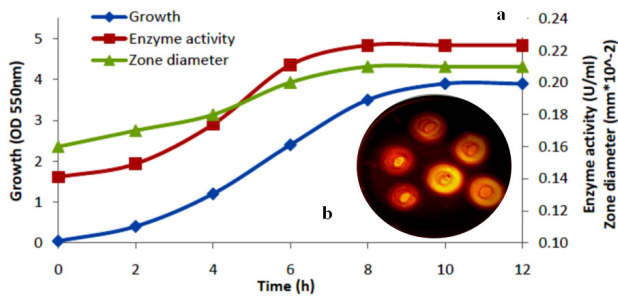
3.2 Optimizing Culture Conditions for Agarase Production Using Plackett-Burman Design

The PB design was utilised to screen the significant factors relevant for agarase production by *Pseudoalteromonas* sp. MHS grown on NB medium supplemented with agar. These factors were yeast, peptone, agar, pH, agitation, inoculum size, and seawater concentration. In this experiment 7 variables were evaluated by 9 experiments and the levels of each variable were determined. The application of statistical design was performed in a 'two-phase' optimization process. The initial step was to look for significant influences on agarase production followed by verification experiment to validate the results under precise, optimised experimental settings. All of the experiments followed a design matrix (Table 1) that was based on the number of variables to be investigated. Each column of the matrix represented an independent variable whose level was varied, and each

row represented a trial. Each variable was evaluated at two levels, a high (+) and a low (–) level [18]. Agarase activity was measured using the DNS assay after 12 h of incubation.

Table 1. Levels of independent factors in the Plackett-Burman design

Variable	−1	0	+1
Yeast (g/L)	1	3	5
Peptone (g/L)	3	5	7
Agar (g/L)	0.5	1	2
Inoculum size (%)	1	2	4
pH	6	7.5	9
Seawater (%)	50	100	100
Agitation	Static	120 rpm	230 rpm

The main effect of each variable upon enzyme activity was valued and presented graphically in Figure 7. As clearly presented from this chart, variables such as pH, agitation, inoculums size, agar, and yeast concentration had positive effects on agarase production while peptone and seawater concentration had negative effects. Therefore, decreasing the peptone and seawater, and simultaneously increasing pH, shaking, inoculum size, agar and yeast can boost productivity of agarase in the culture medium. In agreement with our findings, Fu et al. (2009) [17] used a nine-factor, twelve-run Plackett-Burman design to maximise agarase production by *Agarivorans albus* YKW-34 who stated that, the initial pH had a substantial impact on agarase production ($p < 0.05$). Furthermore, in the Plackett-Burman design, yeast, agar, and starting pH exhibited beneficial impacts (t-value > 0) across the range of examined levels.

Table 2. Plackett-Burman design matrix representing the coded values for 7 independent factors, 0 represents the original concentration, -1 denotes the low level and +1 represents the high level for each component. Enzyme activity was calculated as the response.

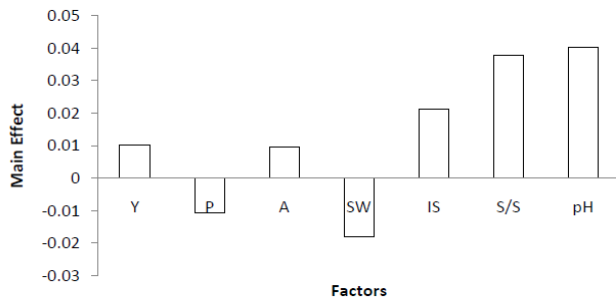| Trial no.	Yeast	Peptone	Agar	Seawater	Inoculum size	Agitation	pH	Enzyme activity (U/mL)
1	−1	−1	−1	1	1	1	−1	0.19
2	−1	−1	1	1	−1	−1	1	0.18
3	−1	1	−1	−1	1	−1	1	0.2
4	−1	1	1	−1	−1	1	−1	0.186
5	1	−1	−1	−1	−1	1	1	0.238
6	1	−1	1	−1	1	−1	−1	0.19
7	1	1	−1	1	−1	−1	−1	0.14
8	1	1	1	1	1	1	1	0.24
9	0	0	0	0	0	0	0	0.22

Figure 7. Main effect of the culture factors that affect agarase production by *Pseudoalteromonas* sp. MHS

The statistical significance of the measured response and evaluated main effects of each variable were determined by statistical analysis of the Plackett-Burman experiment using the t-test provided by Excel Microsoft Office (Table 3).

Table 3. Statistical analysis of the Plackett-Burman experimental results

Factors	Significance level (%)	*P-value*	t-value
Yeast extract	63	0.36185	0.388315
Peptone	65	0.348448	-0.41274
Agar	63	0.362537	0.372091
Seawater	74	0.252522	-0.71774
Inoculum size	78	0.216116	0.853751
Agitation	93	0.062652	1.780418
pH	95	0.04832	1.94318

In the present study, confidence levels of 95% and 93% were reported for pH and agitation respectively. On the other hand, confidence levels lower than 90% were found for inoculum size and seawater concentration of 78% and 74% respectively. Yeast extract, agar and peptone concentrations had confidence levels of 63%, 63% and 65% respectively. The contribution of each factor is represented in the following Pareto chart (Figure 8).
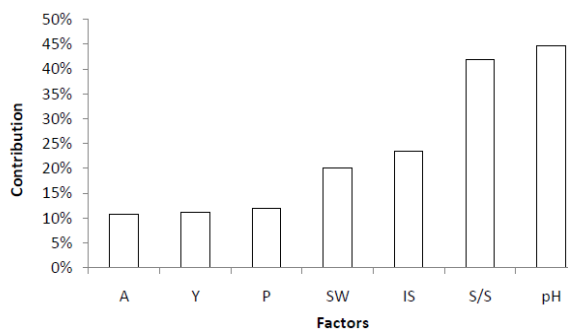

Figure 8. Pareto chart of standardized effects for agarase from *Pseudoalteromonas* sp. MHS after 12 h of cultivation for the Plackett-Burman design.

Verification experiment

To forecast the near-optimal levels of independent variables, a verification experiment was carried out in triplicate. The values of an anti-optimized medium were the polar opposites of those of an optimized one. As we notice from Figure 9, the optimized medium was the preferable medium for agarase production by *Pseudoalteromonas* sp. MHS showing the highest enzyme activity (0.29 U/mL) when cultivated in optimized medium and the lowest (0.14 U/mL) when cultivated in anti-optimized medium while growing in the basal medium showed corresponding agarase activity of 0.22 U/mL.
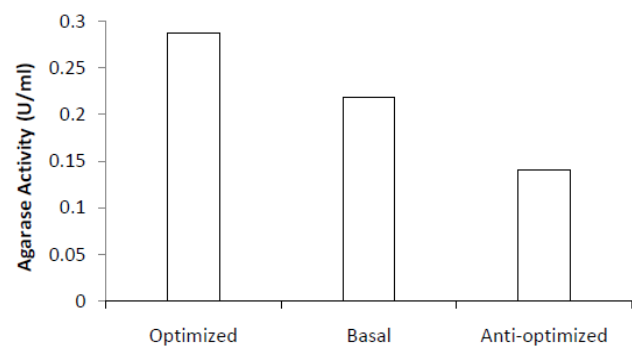
Figure 9. Verification experiment of the applied Plackett-Burman statistical design, comparing agarase activity produced by *P.* sp. MHS grown on optimized, basal, and anti-optimized media for 12 h at 25 °C.

3.3 Purification and Characterization of P. sp. MHS Agarase

3.3.1 Enzyme Purification

Partial purification of the bacterial crude extract was achieved after salting-out with ammonium sulfate followed by enzyme dialysis. Many literature have reported the use of ammonium sulfate in the purification of agarase [24,42,43].

3.3.2 SDS-PAGE of the Enzyme

The partially purified enzyme was subjected to SDS-PAGE that confirmed only one band was observed. The molecular weight (MW) of the protein band was between 15 kDa and 25 kDa (Figure 10).

In accordance to the obtained molecular weight (between 15 kDa and 25 kDa) of the protein band in this work, the reported MW of agarase differs from values as low as 20 kDa for *Bacillus subtilis* [9], to as high as 80 kDa, in the case of *Pseudomonas*-like bacteria [36].

Saraswathi et al. (2011) [9] reported that the molecular weight of purified agarase from *Bacillus subtilis* (20 kDa) was close to those reported for agarases, and in contrast to that produced by *Pseudoalteromonas hodoensis* H7, 35 kDa [11] and *Pseudoalteromonas* sp. NJ21, 80 kDa [36].
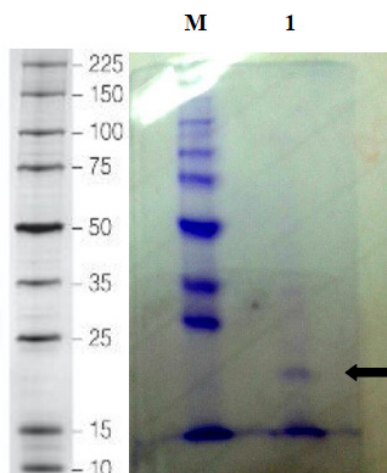

Figure 10. SDS-PAGE analysis of partially purified agarase; Lane M, molecular weight standards; Lane 1 partially purified agarase after $(NH4)_2SO_4$ precipitation

3.3.3 Effect of Temperature on Agarase Activity and Stability

Temperature is thought to be a crucial factor in enzyme activity. Therefore, temperature effects on *P.* sp. MHS agarase activity were investigated by assessing the activity at various temperatures (20 °C-60 °C). As shown in Figure 11a, agarase had a peak temperature of 50 °C and approximately 94% of the supreme activity was detected at 40 °C. When the temperature reached 60 °C, the enzyme had only 87% of its optimal activity whereas, 54% and 82% of the optimal activity were noticed at 20 and 30 °C, respectively. The effect of temperature on the stability of the purified enzyme was studied in the range of 20 °C-60 °C. As noticed from Figure 11b, the stability of the enzyme decreased as the temperature increased; the enzyme could retain about 98%, 90%, 80%, 75%, and 60% of its activity at 20, 30, 40, 50, and 60 °C, respectively.

Because dense bundles of gelled agar inhibit enzyme action, the temperature optima of various agarases are greater than the agar gelling temperature [24]. The optimum temperature of 50 °C for *Pseudoalteromonas* sp. MHS agarase is similar to that of agarase-b produced by *Agarivorans albus* OAY02 [34], less than that of 60 °C for *Catenovulum agarivorans* YM01T agarase [25], and higher than that of 30 °C for *Pseudoalteromonas* sp. NJ21 agarases [36], 35 °C of *Agarivorans* sp. JA-1 agarase [44],

40 °C of agarase-a from *Agarivorans albus* OAY02 [34], and 45 °C of *Pseudoalteromonas hodoensis* H7 agarase [11]. The increased thermostability of *Pseudoalteromonas* sp. MHS will be beneficial for industrial applications.
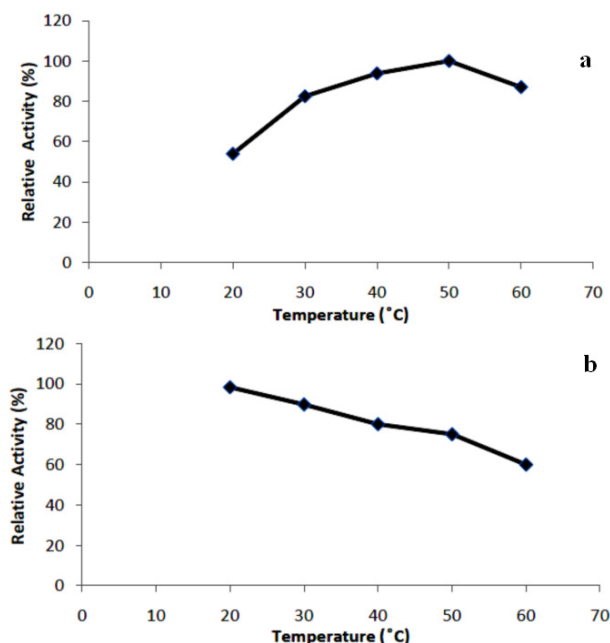
Figure 11. Effect of different temperatures on agarase activity (a) and stability (b)

3.4 The Use of Red Seaweed Pterocladia capillacea as Substrate for Agarase Production

While chemical degradation of biomass is a faster and less expensive choice, it has a number of drawbacks, including the production of toxic waste that is harmful to the environment and toxic end products that are not fermentable. Developing an appropriate enzymatic method for biomass degradation is becoming increasingly crucial in this regard. The isolation of microorganisms with strong biopolymer hydrolyzing activity is critical for the successful development of marine biomass for industrial use. Due to its employment as an industrial resource and a depolluting plant for cleaning inland sea areas and eutrophied seawater, the amount of seaweed trash is steadily increasing [45]. As a result, the recycling of organic substances and the protection of the marine environment needs the utilisation of seaweed waste [46,47].

Therefore, in this experiment, it was aimed to produce agarase from a low cost substrate for economic purposes. The red seaweed *Pterocladia capillacea* was used as a natural medium with no additives for the growth of *Pseudoalteromonas* sp. MHS. Figure 12a illustrates the medium prepared with the 20 g/L *Pterocladia capillacea* in seawater after autoclaving while Figure 12b illustrates

the liquefaction of algal biomass after inoculation by *Pseudoalteromonas* sp. MHS and incubation at 25 °C and 230 rpm for 24 h.
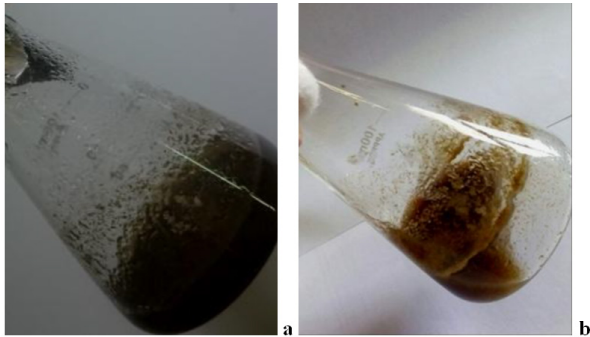

Figure 12. Twenty g/L *Pterocladia capillacea* in seawater after autoclaving (a), and medium liquefaction by *Pseudoalteromonas* sp. MHS grown at 25 °C and 230 rpm for 24 h (b)

Data in Table 4 depict that an activity of 0.27 U/mL of agarase was obtained after 12 h of incubation for the three different concentrations of the seaweed used. However, the flask containing the highest concentration of the seaweed (20 g/L) was only partially liquefied by the bacterium and the enzyme activity couldn't be measured due to its high viscosity. Consequently, measurements taken after 24 h of incubation were higher compared to those taken after 12 h.

Table 4. Agarase activity of *P.* sp. MHS grown on red seaweed

Seaweed conc. (g/L)	Incubation Time (h)	
	12	24
	Enzyme activity (U/mL)	
5	0.27	0.26
10	0.27	0.3
15	0.27	0.31
20	*Nd	0.35

*Nd: Not determined

It is worth to mention that the agarase activities recorded after 24 h of incubation (0.3, 0.31, and 0.35 U/mL) using 10, 15, and 20 g/L of biomass, respectively were higher than that of 0.29 U/mL obtained from the optimized medium of PB design. This indicates that red seaweeds could replace media used for agarase production and are suitable sources for bacterial nutrition.

According to the findings of this study, red algae of the genus *Pterocladia* are often found in the seas of Lebanon, Egypt, Brazil, Italy, and other countries for the industrial production of gelling galactans [48,49]. Red seaweed has a carbohydrate composition of 30%-60%,

with agar and carrageenan accounting for the majority of it. Unused seaweed trash is commonly disposed of via landfill, incineration, or dumping into the sea, all of which pollute the environment. Kang & Kim (2015) [46] isolated a *Bacillus* sp. SYR4 strain that was able to use seaweed waste as a carbon source by degrading both agar and carrageenan and producing reducing sugars, which served as a substrate for bioethanol production, yielding 7-10 wt% ethanol [50].

4. Conclusions and Future Perspectives

This study provides evidence that marine bacteria, particularly those associated with algae contribute in the production of hydrolytic enzymes such as agarase. The study evaluated a strain of *Pseudoalteromonas* sp. MHS isolated from the green alga *Ulva lactuca* to produce agarase and degrade agar. Agarase activity was optimized via an experimental Plackett-Burman design. The utilization of red algae that usually disposed in the environment as substrate for agarase production was examined for an economic purpose. Surprisingly the activity obtained was higher than that recorded with microbiological media. We therefore recommend the use of the huge amount of seaweeds disposed in the environment as substrate for microbial production of enzymes. Although agarases have an old history of application in various industries, they are still in the experimental stages and are not commercially available. Therefore, they are expected to increase further study in the very near future thereby leading to further advancement in the biotechnology fields.

Author Contributions

M.M.S. conceived and conducted the experiments; S.S.A. conceived the idea, analyzed and interpreted the data, wrote the manuscript; M.E.M., H.A.G., and S.A.S. conceived the research idea, analyzed the data, and edited the manuscript.

Competing Interests

The authors declare no competing interests.

Data Availability Statement

Correspondence and requests for materials should be addressed to S.S.A. The datasets generated and analyzed during the current study are available from the corresponding author on reasonable request.

References

[1] Comba-González, N.B., Ruiz-Toquica, J.S., López-

Kleine, L., Montoya-Castaño, D., 2016. Epiphytic bacteria of macroalgae of the Genus *Ulva* and their potential in producing enzymes having biotechnological interest. Mar Biol Oceanogr. 5, 1-9.

[2] Song, T., Zhang, W., Wei, C., Jiang, T., Xu, H., Cao, Y., Cao, Y., Qiao, D., 2015. Isolation and characterization of agar-degrading endophytic bacteria from plants. Curr. Microbiol. 70, 275-281.

[3] Seok, J.H., Kim, H.S., Hatada, Y., Nam, S.W., Kim, Y.H., 2012. Construction of an expression system for the secretory production of recombinant α-agarase in yeast. Biotechnol. Lett. 34, 1041-1049.

[4] Popper, Z.A., Michel, G., Hervé, C., Domozych, D.S., Willats, W.G., Tuohy, M.G., Kloareg, B., Stengel, D.B., 2011. Evolution and diversity of plant cell walls: from algae to flowering plants. Annu. Rev. Plant Biol. 62, 567-590.

[5] Martin, M., Barbeyron, T., Martin, R., Portetelle, D., Michel, G., Vandenbol, M., 2015. The cultivable surface microbiota of the brown alga *Ascophyllum nodosum* is enriched in macroalgal-polysaccharide-degrading bacteria. Front Microbiol. 6, 1487.

[6] Martin, M., Portetelle, D., Michel, G., Vandenbol, M., 2014. Microorganisms living on macroalgae: diversity, interactions, and biotechnological applications. Appl. Microbiol. Biotechnol. 98, 2917-2935.

[7] Trincone, A., 2011. Marine Biocatalysts: Enzymatic features and applications. Mar. Drugs. 9, 478-499.

[8] Chi, W.J., Chang, Y.K., Hong, S.K., 2012. Agar degradation by microorganisms and agar-degrading enzymes. Appl. Microbiol. Biotechnol. 94, 917-930.

[9] Saraswathi, S., Vasanthabharathi, V., Kalaiselvi, V., Jayalakshmi, S., 2011. Characterization and optimization of agarase from an estuarine *Bacillus subtilis*. Microbiol. Res. 5, 2960-2968.

[10] Ziayoddin, M., Lalitha, J., Shinde, M., 2014. Optimization of agarase production by alkaline *Pseudomonas aeruginosa* ZSL-2 using Taguchi experimental design. ILNS. 12, 180-193.

[11] Chi, W., Park, J., Kang, D., Hong, S., 2014. Production and characterization of a novel thermostable extracellular agarase from *Pseudoalteromonas hodoensis* newly isolated from the west sea of South Korea. Appl. Biochem. Biotechnol. 173, 1703-1716.

[12] Choi, H.J., Hong, J.B., Park, J.J., Chi, W.J., Kim, M.C., Chang, Y.K., Hong, S.K., 2011. Production of agarase from a novel *Micrococcus* sp. GNUM-08124 strain isolated from the East Sea of Korea. Biotechnol. Bioprocess Eng. 16, 81.

[13] Temuujin, U., Chi, W.J., Chang, Y.K., Hong, S.K., 2012. Identification and biochemical characterization of Sco3487 from *Streptomyces coelicolor* A3(2), an exo and endo-type β-agarase-producing neoagarobiose. Bacteriol. 194, 142-149.

[14] Wu, H., Chen, G., Bian, Y., Zeng, W., Sun, B., Liang, Z., 2017. Identification and characterization of a new agar-degrading strain with the novel properties of saccharides inhibition and nitrogen fixation. Microbiol. 55, 475-482.

[15] Abouelkheir, S.S., Abdelghany, E.A., Ghozlan, H.A., Sabry, S.A., 2020. Characterization of Biofilm Forming Marine *Pseudoalteromonas* spp. J. Mar. Sci. 2(1), 31-37.

[16] Abouelkheir, S.S., Abdelghany, E.A., Sabry, S.A., Ghozlan, H.A., 2021. Biofilm Formation by Marine *Cobetia marina* alex and *Pseudoalteromonas* spp: Development and Detection of Quorum Sensing N-Acyl Homoserine Lactones (AHLs) Molecules. Mar. Sci. 3(3), 1-12.
DOI: https://doi.org/10.30564/jms.v3i3.3397.

[17] Fu, X.T., Lin, H., Kim, S.M., 2009. Optimization of medium composition and culture conditions for agarase production by Agarivorans albus YKW-34. Process Biochem. 44, 1158-1163.

[18] Gu, W.X., Chen, Y.L., Niu, H.N., Lu, X., Mao, X.Z., Du, Z.J., Liu, X.L., 2012. Enhanced Activity of Intracellular Agarase from a Novel Marine Strain *Agarivorans gilvus* WH0801. In Adv. Mater. Res. Trans Tech Publications, Ltd. 554-556, 1227-1232.
DOI: https://doi.org/10.4028/www.scientific.net/amr.554-556.1227

[19] Jung, C., Kwon, H., Park, C., Lee, J., 2012. Optimization of *Pseudoalteromonas* sp. JYBCL 1 culture conditions, medium composition and extracellular β-agarase activity. Biotechnol. Bioprocess Eng. 17, 937-945.

[20] Saqib, A.A., Whitney, P.J., 2011. Differential behaviour of the dinitrosalicylic acid (DNS) reagent towards mono- and di-saccharide sugars. Biomass and Bioenergy. 35(2011), 4748-4750.

[21] Calissendorff, J., Falhammar, H., 2017. Lugol's solution and other iodide preparations: perspectives and research directions in Graves' disease. Endocrine. 58, 467-473.
DOI: https://doi.org/10.1007/s12020-017-1461-8

[22] https://www.bio-rad.com/webroot/web/pdf/lsr/literature/Bulletin_6040.pdf.

[23] Faturrahman, F., Meryandini, A., Junior, M.Z., Rusmana, I., 2011. Isolation and identification of an agar-liquefying marine bacterium and some properties of its extracellular agarases. Biodiversitas. 12, 192-197.

[24] Feng, Z., Li, M., 2013. Purification and characterization of agarase from *Rhodococcus* sp. Q5, a novel

agarolytic bacterium isolated from printing and dyeing wastewater. Aquaculture. 372, 74-79.

[25] Cui, F., Dong, S., Shi, X., Zhao, X., Zhang, X., 2014. Overexpression and characterization of a novel thermostable β-Agarase YM01-3, from marine bacterium *Catenovulum agarivorans* YM01T. Mar. Drugs. 12, 2731-2747.

[26] Furusawa, G., Lau, N.S., Suganthi, A., Amirul, A.A.A., 2017. Agarolytic bacterium *Persicobacter* sp. CCB-QB2 exhibited a diauxic growth involving galactose utilization pathway. Microbiologyopen. 6, 1-11.

[27] Moyes, R.B., Reynolds, J., Breakwell, D.P., 2009. Differential staining of bacteria: negative stain. Curr. Protoc. Microbiol. A-3F. John Wiley & Sons, Inc.

[28] Duguid, J.P., 1951. The demonstration of bacterial capsules and slime. Pathol. 63, 673-685.

[29] Buck, J.D., 1982. Nonstaining (KOH) method for determination of gram reactions of marine bacteria. Appl. Environ. Microbiol. 44, 992-993.

[30] Phanse, N., Chincholikar, A., Patel, B., Rathore, P., Vyas, P., Patel, M., 2011. Screening of PHA (poly hydroxyalkanoate) producing bacteria from diverse sources. Biosci. 1, 27-32.

[31] Sambrook, J., Fritsch, E.F., Maniatis, T., 1989. Molecular cloning: a laboratory manual (No. Ed. 2). Cold spring harbor laboratory press.

[32] Saravanan, D., Kumar, V.K., Radhakrishnan, M., 2015. Isolation and optimization of agarase producing bacteria from marine sediments. Chem. Tech. Res. 8, 1701-1705.

[33] Deshavath, N.N., Mukherjee, G., Goud, V.V., Veeranki, V.D., Sastri, C.V., 2020. Pitfalls in the 3, 5-dinitrosalicylic acid (DNS) assay for the reducing sugars: Interference of furfural and 5-hydroxymethylfurfural. Int. J. Biol. Macromolecules, 156 (2020) xxx. https://www.researchgate.net/deref/https%3A%2F%2Fdoi.org%2F10.1016%2Fj.ijbiomac.2020.04.045.

[34] Yang, M., Mao, X., Liu, N., Qiu, Y., Xue, C., 2014. Purification and characterization of two agarases from *Agarivoransalbus* OAY02. Process Biochem. 49, 905-912.

[35] Plackett, R.L., Burman, J.P., 1946. The design of optimum multifactorial experiments. Biometrika. 33, 305-325.

[36] Li, J., Hu, Q., Li, Y., Xu, Y., 2015. Purification and characterization of cold-adapted beta-agarase from an Antarctic psychrophilic strain. Braz J Microbiol. 46, 683-690.

[37] Liu, Y., Tian, X., Peng, C., Du, Z., 2019. Isolation and Characterization of an Eosinophilic GH 16 β-Agarase (AgaDL6) from an Agar-Degrading Marine Bacterium *Flammeovirga* sp. HQM9. Microbiol. Biotechnol. 29(2), 235-243.
DOI: https://doi.org/10.4014/jmb.1810.09065

[38] Rhee, Y.J., Han, C.R., Kim, W.C., Jun, D.Y., Rhee, I.K., Kim, Y.H., 2010. Isolation of a novel freshwater agarolytic Cellvibrio sp. KY-YJ-3 and characterization of its extracellular beta-agarase. Microbiol. Biotechnol. 20, 1378-1385.

[39] Oh, Y.H., Jung, C., Lee, J., 2011. Isolation and characterization of a novel agarase- producing *Pseudoalteromonas* spp. bacterium from the guts of spiny turban shells. Microbiol. Biotechnol. 21, 818-821.

[40] Kim, J., Hong, S.K., 2012. Isolation and characterization of an agarase-producing bacterial strain, *Alteromonas* sp. GNUM-1, from the West Sea, Korea. Microbiol. Biotechnol. 22, 1621-1628.

[41] Egan, S., Holmström, C., Kjelleberg, S., 2001. *Pseudoalteromonas ulvae* sp. nov., a bacterium with antifouling activities isolated from the surface of a marine alga. Syst. Evol. Microbiol. 51, 1499-1504.

[42] Song, T., Cao, Y., Xu, H., Zhang, W., Fei, B., Qiao, D., Cao, Y., 2014. Purification and characterization of a novel β-agarase of *Paenibacillus* sp. SSG-1 isolated from soil. Biosci. Bioeng. 118, 125-129.

[43] Li, J., Sha, Y., Seswita-Zilda, D., Hu, Q., He, P., 2014. Purification and characterization of thermostable Agarase from *Bacillus* sp. BI-3, a thermophilic bacterium isolated from Hot Spring. Microbiol. Biotechnol. 24, 19-25.

[44] Lee, D.G., Jeon, M.J., Lee, S.H., 2012. Cloning, expression, and characterization of a glycoside hydrolase family 118 beta-agarase from *Agarivorans* sp. JA-1. Microbiol. Biotechnol. 22, 1692-1697.

[45] Tang, J., Wang, M., Zhou, Q., Nagata, S., 2011. Improved composting of *Undaria pinnatifida* seaweed by inoculation with *Halomonas* and *Gracilibacillus* sp. isolated from marine environments. Bioresour. Technol. 102, 2925-2930.

[46] Kang, S., Kim, J.K., 2015. Reuse of red seaweed waste by a novel bacterium, *Bacillus* sp. SYR4 isolated from a sandbar. Microbiol. Biotechnol. 31, 209-217.

[47] Abouelkheir, S.S., Kamara, M.S., Atia, S.M. et al., 2020. Novel research on nanocellulose production by a marine *Bacillus velezensis* strain SMR: a comparative study. Sci Rep. 10, 14202.
DOI: https://doi.org/10.1038/s41598-020-70857-7

[48] Silva, L.M.C.M., Lima, V., Holanda, M.L., Pinheiro, P.G., Rodrigues, J.A.G., Lima, M.E.P., Benevides, N.M.B., 2010. Antinociceptive and Anti-inflammatory Activities of Lectin from Marine Red Alga *Pterocladiella capillacea*. Biol. Pharm. Bull. 33, 830-835.

[49] Sebaaly, C., Karaki, N., Chahine, N., Evidente, A., Yassine, A., Habib, J., Kanaan, H., 2012. Polysaccharides of the red algae ―*Pterocladia*"growing on the Lebanese coast: Isolation, structural features with antioxidant and anticoagulant activities. J App Pharm Sci. 2, 1-10.

[50] Chauhan, P.S., Saxena, A., 2016. Bacterial carrageenases: an overview of production and biotechnological applications. 3 Biotech. 6, 1-18.

ARTICLE

Hydrodynamic Performance of Open-frame Deep Sea Remotely Operated Vehicles Based on Computational Fluid Dynamics Method

Qianrong Li[1]   Baoji Zhang[2*]

1. Merchant Marine College, Shanghai Maritime University, Shanghai, 201306, China
2. College of Ocean Science and Engineering, Shanghai Maritime University, Shanghai, 201306, China

ARTICLE INFO	ABSTRACT

The resistance performance and motion stability of deep sea remotely operated vehicles (ROVs) subjected to underwater motion conditions are studied on the basis of the unsteady Reynolds-averaged Navier-Stokes method combined with the six-degree-of-freedom equation of motion to quickly and accurately predict them. In the modeling process, we consider the complexity of ROV geometry and thus reduce the model to a series of regular geometries to maximize the position and weight of the original components. The grid and value slots of an ROV are divided, and the surface is reconstructed. The forward, backward, transverse, floating, and submerged resistance of ROVs are simulated and compared with existing experimental forces to determine the accuracy of the calculation method. Then, the oblique navigation of the ROV on the horizontal and vertical planes is studied. Furthermore, the motion response of the ROV to direct horizontal motion, heave, pitch, and yaw are studied. The force, moment, and motion time curves are obtained. The stability of ROV motion is analyzed to provide technical support for the safety of ROVs.

1. Introduction

Remotely operated vehicles (ROVs) are unmanned underwater vehicles with acoustic and optical sense systems. An umbilical cable is used in ROVs to provide energy and transmit signals by remote control. It can accomplish high-intensity and high-load work under complex sea conditions and can be used in many fields, such as oceanographic survey, pipeline inspection, and offshore structural maintenance. In the development of

ROVs and in actual operations, their safety and stability are important considerations, and their resistance characteristics are the premise and basis of ROV motion stability. Therefore, the resistance characteristics of ROVs should be accurately predicted to build a foundation for ROV motion control. At present, the methods for accurately obtaining the hydrodynamic performance of ROVs subjected to underwater motion include the captive mode test method and computational fluid dynamics

*Corresponding Author:

Baoji Zhang,

College of Ocean Science and Engineering, Shanghai Maritime University, Shanghai, 201306, China;

Email: zbj1979@163.com

(CFD) numerical simulation method. The captive mode test method mainly includes the linear resistance test, spiral arm test, circular motion test, and plane motion mechanism (PMM) test, which is currently the most widely used in testing hydrodynamic performance. Zhang et al. (2010) [1] took an open-frame ROV as the research object and obtained the hydrodynamic coefficient with the captive mode test method. Juan et al. (2011) [2] used PMM technology to perform a concussion test on a full-scale open-frame ROV and compared the test results with the results of the Morison equation. Fan and Lian (2012) [3] used a large-amplitude horizontal PPM to conduct an in-plane oblique navigation test on a deep-sea ROV and obtained the hydrodynamic coefficient via multiple regression.

Although the captive mode test method achieves certain accuracy, it is not conducive to the development and design of low-cost ROVs due to the long test time and high cost. With the rapid development of computer technology, CFD methods can be used to predict the hydrodynamic performance of ROVs as they have become a common method in the early design stage of ROVs. Leong et al. (2015) [4] developed a numerical model to predict the pure sway motion of an underwater vehicle at different lateral and longitudinal positions relative to a large underwater vehicle using the CFD method. Kang et al. (2005) [5] used CFD software to simulate the periodic heave motion of an underwater submersible body and compared the obtained data with the model test results. Alexander et al. (2007) [6] used CFD software to study the resistance performance of underwater robots. The calculation results are consistent with the experimental data. Zhang et al. (2010) [7] calculated the hydrodynamic coefficient for a long-endurance underwater vehicle. Wang et al. (2011) [8] took a five-degree-of-freedom disc-shaped underwater robot as the research object and used CFD software to calculate the resistance. Chin and Lau (2012) [9] used the CFD software ANSYS-CFX to calculate the hydrodynamic performance of a complex-shaped ROV system and verified the theoretical calculations through model tests. Nedelcu et al. (2018) [10] provided a model used for simulation and modeling to obtain the hydrodynamic characteristics of an ROV using ANSYS-CFX. Badawy et al. (2013) [11] calculated hydrodynamic coefficients using the CFD software ANSYS-CFX. The numerical simulation is in good agreement with the experimental data. José et al. (2015) [12] used ANSYS-CFX software to calculate the drag coefficient of an ROV. Wang et al. (2014) [13] developed a mathematical model of an underwater vehicle based on CFD calculations, strip theory, and open-water tests. Skorpa (2002) [14] simplified

an open-frame ROV and used different turbulence models to study the wake distribution of the ROV during underwater motion. Vaz et al. (2010) [15] compared two viscous solvers for the accurate prediction of the maneuvering forces of streamlined submersibles using CFD calculations and so on. Yu et al. (2018) [16] calculated the hydrodynamic performance of a six-degree-of-freedom (6DOF) ROV under different working conditions on the basis of the CFD method. Chin et al. (2018) [17] used STAR CCM+™ and WAMIT™ to compute the hydrodynamic damping coefficients and added mass coefficients of an ROV. Andra et al. (2018) [18] conducted a CFD analysis for an ROV in a horizontal plane for different velocities to obtain the hydrodynamic force characteristics. Tadeusz et al. (2018) [19] used CFD to calculate the pressure of the propeller of an ROV and thereby optimize its propulsion. Juan et al. (2016) [20] used a viscous flow solver to accurately predict the maneuverability coefficient of an ROV. Christian et al. (2013) [21] analyzed the hydrodynamic behavior of an ROV under different flow conditions. The results of the model show good agreement with those in published research. Hung et al. (2013) [22] presented a numerical simulation of a recently developed ROV utilizing theoretical and experimental work to obtain the vehicle's hydrodynamic coefficients and a Laboratory Virtual instrument Engineering Workbench (LabVIEW) based numerical model to predict its behavior. Lau et al. (2008) [23] proposed a new experimental method to determine the added mass and drag coefficients of an ROV on the basis of the classical free decay test; the experiment results agreed with those of the CFD program. Muljowidodo et al. (2009) [24] used CFD to identify the fluid characteristics on a thruster. James et al. (2014) [25] presented a methodology to increase an ROV's capabilities by optimizing its drag profile through a combination of CFD modeling and subscale experiments. Collectively, the existing studies on the hydrodynamics performance of ROVs at home and abroad mainly focus on the calculation of the simplified open-frame ROV resistance. Studying the stability of ROVs requires the accurate prediction of their hydrodynamic performance. Therefore, the current work summarizes previous research results on the basis of a deep sea ROV model and simulates the forward, backward, transverse, floating, and submerged resistance of the ROV with the Reynolds-averaged Navier-Stokes (RANS) method. The results are compared with the experimental outcomes. The resistance of the ROV under direct horizontal navigation and that under oblique navigation are studied. Then, the motion responses of the ROV under direct horizontal motion, heave, pitch, and yaw are studied with a 6DOF equation

to obtain the corresponding force and moment curves. The stability of ROV motion is analyzed to provide technical support for the safety of ROV.

2. Theoretical Background

The CFD technique is used to assist in the calculation of ROV resistance. The turbulent flow field around the ROV is analyzed with the general CFD software STAR CCM^{+TM}.

2.1 Control Equation

The whole flow field uses the continuity equation and RANS equations as the governing equations (2017) [26].

$$\frac{\partial U_i}{\partial x_i} = 0 \qquad (1)$$

$$\rho \frac{\partial U_i}{\partial t} + \rho U_j \frac{\partial U_i}{\partial x_j} = -\frac{\partial \hat{p}}{\partial x_i} + \frac{\partial}{\partial x_j}(\mu \frac{\partial U_i}{\partial x_j} - \rho \overline{u_i u_j}) + f_i^* \qquad (2)$$

where $U_i=(U,V,W)$ is the velocity component in the $x_i=(x, y, z)$ direction; ρ, $\hat{p}$, μ, $-\rho \overline{u_i u_j}$, and f_i^* are the fluid density, static pressure, fluid viscosity, Reynolds stresses, and body forces per unit volume, respectively.

2.2 Turbulence Model

The turbulence model adopts the renormalization group $k - \hat{a}$ model, and the forms of the turbulence energy transport equation and energy dissipation transport equation are as follows (2017) [27].

$$\rho \frac{dk}{dt} = \frac{\partial}{\partial x_i}\left[(\alpha_k \mu_{eff})\frac{\partial k}{\partial x_i}\right] + G_k + G_b - \rho\varepsilon - Y_M \qquad (3)$$

$$\rho \frac{d\varepsilon}{dt} = \frac{\partial}{\partial x_i}\left[(\alpha_\varepsilon \mu_{eff})\frac{\partial \varepsilon}{\partial x_i}\right] + C_{1\varepsilon}\frac{\varepsilon}{k}(G_k + C_{3\varepsilon}G_b) - C_{2\varepsilon}\rho\frac{\varepsilon^2}{k} \qquad (4)$$

where μ_{eff} is the effective dynamic viscosity; and k and ε are the turbulent kinetic energy and turbulent dissipation rate, respectively. G_k is the generation of turbulent kinetic energy by the mean velocity gradients. G_b is the generation of turbulent kinetic energy by buoyancy. Y_M represents the contribution of the fluctuating dilatation to compressible turbulence. $C_{1\varepsilon}$, $C_{3\varepsilon}$, and $C_{2\varepsilon}$ are empirical constants.

2.3 Motion Equation of ROV

While establishing the motion equation of the ROV, we establish two reference coordinate systems (Figure 1). One is a fixed coordinate system $O_oX_oY_oZ_o$ fixed on the earth; the other is a moving system OXYZ fixed on the ROV. The origin of the moving coordinate system is located at the center of mass of the ROV. The motion

equations can be written as (2005) [28].

$$\frac{dB}{dt} + \Omega \times B = F \qquad (5)$$

$$\frac{dK}{dt} + \Omega \times K + U \times B = M \qquad (6)$$

where B is the momentum of ROV, Ω is the angular velocity, F is the external force, and K is the moment of momentum. U is the speed of the ROV, and M is the resultant moment.
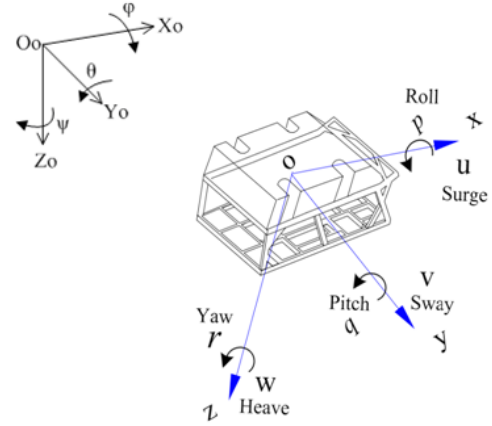

Figure 1. CAD SolidWorks model for ROV and its body-fixed coordinate system

3. ROV Model

The principal dimension and related parameters of the model are shown in Table 1. The scale ratio of the model is 1:1.6. The upper part of the main hull is buoyant material, the lower part of the truss is made of steel, and the other parts are simplified.

Table 1. Parameters of ROV model

Parameter	Unit	Value
Length of ROV model (L)	m	1.88
Width of ROV model (B)	m	1.13
Height of ROV model (H)	m	1.06
Mass of ROV model (M)	Kg	500
Moments of inertia relative to the x axis (I_x)	kg.m^2	264
Moments of inertia relative to the y axis (I_y)	kg.m^2	450
Moments of inertia relative to the z axis (I_z)	kg.m^2	450
Center of gravity of ROV (x_G,y_G,z_G)	M	(0.94,0.185,0.28)

3.1 Computation Domain and Boundary Conditions

The computation domain and boundary conditions are roughly shown in Figure 2. Let the length of the ROV flow direction be L. The length from the inlet to the front of the body is 3.5 L, the length from the rear to the

outlet of the body is 7.5 L. The height and width of the calculation domain are both 3.5 L. The inlet conditions are determined by flow velocity. The outlet conditions are given on the convection of the vertical and horizontal planes of symmetry.
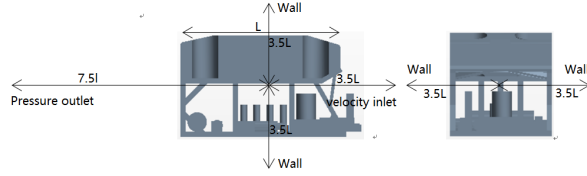

Figure 2. Computing domain and boundary conditions
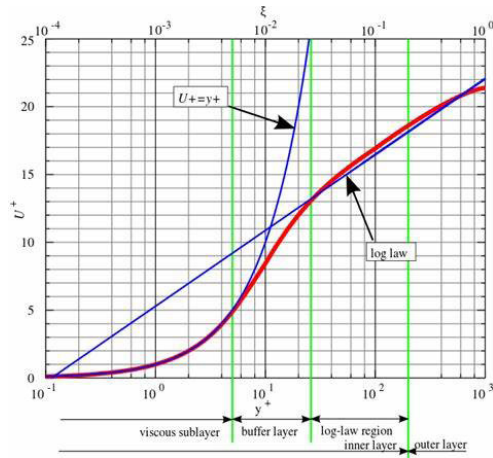
3.2 Near Wall Modeling

Figure 3. Law of the Wall (1995) [29]

To solve the turbulence problem in this work, we use the near wall model for the near-wall region of the ROV. The estimation of the first cell size y is based on the ITTC (International Towing Tank Conference) standard method and is given in the function of the non-dimensional wall distance y^+ and the local Reynolds number R_e of the ROV.

The expression for y^+ coefficient is

$$y^+ = \rho u_T \frac{y}{\mu} \tag{7}$$

where u_T is the velocity friction defined as

$$u_T = \sqrt{\tau_w / \rho} \tag{8}$$

$$y = \frac{y^+ L}{R_e \sqrt{C_f / 2}} \tag{9}$$

$$C_f = \frac{0.075}{(\log_{10} R_e - 2)^2} \tag{10}$$

where L is the length of the ROV and Cf is the friction drag coefficient of the plate.

The y^+ variations of the ROV model for U=1.0 m/s

are presented in Figure 4. The precision of the y^+ values of the ROV determines the quality of the boundary layer solution that affects the friction force. The range of the y^+ values is $0.1 < y^+ < 40$.
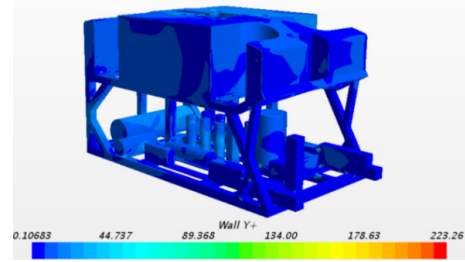
Figure 4. Wall y^+ coefficient of ROV

3.3 Meshing

The whole calculation domain is meshed through body mesh division with right angle cutting. Given that the size of the original model is large and considering the limitation of calculation time and computer performance, we adopt a sparse grid size for the watershed and encrypt the grid only near the ROV. The final number of meshes is 5.46 million. Figures 5 and 6 indicate that the mesh near the ROV is locally refined. For calm water resistance predictions, the time step size is set to be 0.005 ∗ *L*/U.

Figure 5. ROV meshing

Figure 6. Grid horizontal section meshing of ROV

4. Convergence Analysis of CFD Calculation Results

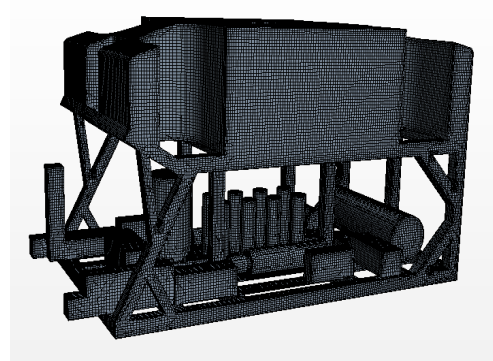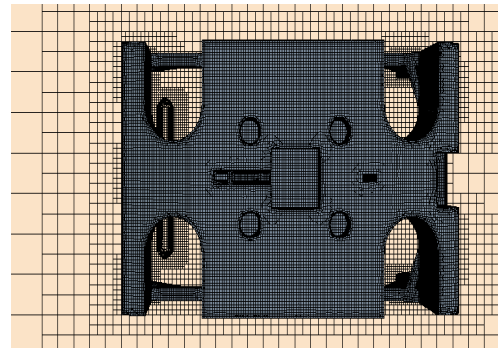The uncertainty of CFD simulation results determines the usefulness of data. Comparing the results obtained by different researchers using different evaluation methods is difficult. Therefore, the CFD uncertainty analysis becomes an important task in CFD research and applications (2012) [30]. This section analyzes the uncertainty of CFD according to the ITTC regulation, that is, verification and validation.

4.1 Verification

In this section, the cutting volume mesh is selected as a case to analyze the uncertainty of the longitudinal resistance of the ROV during direct horizontal navigation. Three grid models are established with the grid refinement ratio $r_G=1.414$. The free surface mesh and waveform diagram are shown in Table 2.
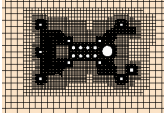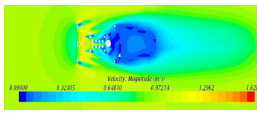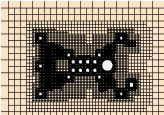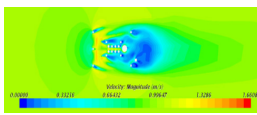
Table 2. Meshing and section pressure
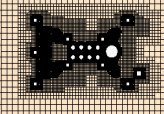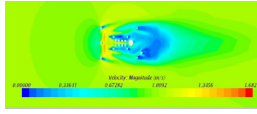
Mesh configuration	Horizontal mesh distribution	Section speed (m/s)
Coarse mesh		
Middle mesh		
Dense mesh		

Table 2 indicates that the three grids clearly present speed cloud maps. The speed of the coarse mesh near the ROV is uneven, and the velocity cloud map obtained by the finely encrypted mesh is relatively uniform.

The error E is defined in Equation (11).

$$E(\%) = \left(\frac{D-S}{D}\right) \times 100 \tag{11}$$

The grid convergence ratio is expressed by the definition in Equation (12).

$$R_G = \frac{\varepsilon_{21}}{\varepsilon_{23}} \tag{12}$$

where $\varepsilon_{21}=S_2-S_1$ and $\varepsilon_{32}=S_3-S_2$. The precision order P_G,

correction factor C_G, and grid uncertainty U_G are defined as follows:

$$P_G = \frac{\ln(\varepsilon_{32}/\varepsilon_{21})}{\ln(r_G)} \tag{13}$$

$$C_G = \frac{r_G^{P_G}-1}{r_G^{P_{th}}-1} \tag{14}$$

$$U_G = \left|C_G \frac{\varepsilon_{21}}{(r_G^{P_G}-1)}\right| + \left|(1-C_G)\frac{\varepsilon_{21}}{(r_G^{P_G}-1)}\right| \tag{15}$$

where the precision limit order (P_{th}) in Equation (14) is 2.0, which is the formal order of CFD code precision. The longitudinal resistance coefficients calculated from the three sets of meshes are shown in Table 3. The longitudinal resistance calculation results are especially accurate when the mesh is encrypted. Table 4 shows the verification of longitudinal resistance coefficient C_{QT}, including the convergent rate R_G, order of accuracy P_G, correction factor C_G, grid spacing uncertainty U_G, error σ^*_{GI} with a corrected factor, corrected uncertainty value U_{GC}, and reference value for corrected numerical simulation S_C. The convergence rate $R_G <1$ indicates that the mesh monotonically converges. The reference value for the corrected numerical simulation S_C is 0.281, which shows that the corrected longitudinal resistance is close to the experimental value with the error of 1.08%.

Table 3. Longitudinal resistance coefficient of three sets of meshes ($C_{QT} \times 10^{-3}$)

Scalar	Coarse (S_3)	Medium (S_2)	Fine (S_1)	Exp. (D)
C_{QT}	0.306	0.287	0.284	0.278
E%D	−10.07	−3.24	−2.16	-

Table 4. Verification of calculation of total resistance coefficient

Mesh configuration	R_G	P_G	C_G	U_G	σ^*_{GI}	U_{GC}	S_C
Cutting volume mesh	0.157	5.328	5.336	0.00544	0.003	0.00244	0.281

4.2 Validation

Validation is the process of using experimental values to evaluate the modeling uncertainty U_{SM} of numerical simulations. If the conditions permit, then the model error σ_{SN} needs to be estimated. Validation determines whether verification is achieved by comparing the errors and confirming the magnitude of uncertainty. If the comparison error is less than the confirmation uncertainty, then the level of confirmation of uncertainty is achieved. The longitudinal resistance confirmation results of three

sets of meshes are shown in Table 5. |E| is less than the uncertainty U_V; thus, the calculation results can be confirmed.

Table 5. Validation of results

Error	Results	Confirmed uncertainty	Result	Relationship of sizes
E_1	0.00552	U_{V1}	0.00775	$|E_1| < U_{V1}$
E_{C1}	−0.00499	U_{V1C}	0.00603	$|E_{C1}| < U_{V1C}$

5. Results Analysis

5.1 Resistance Analysis of ROV during Direct Navigation

The upstream boundary is used as the velocity inlet, the downstream boundary is used as the free outlet, the surrounding boundary and model are used as walls, and simulation is performed using STAR CCM^{+TM} software. The turbulence model is a standard k-ε model. The SIMPLE(Semi-Implicit Method for Pressure Linked Equations) algorithm is used to solve the pressure-velocity coupled equations. The finite difference method is used to discretize the algebraic equations. The momentum, turbulent kinetic energy, and turbulent dissipation rate are discretized using the first-order difference scheme. The calculation speed is 0.2-1.0 m/s.

The resistance of the forward, backward, left shift, right shift, down shift, and up shift motions of the ROV at different speeds is simulated, and the numerical calculation results are compared with the test results (Fan, 2013). Table 6 shows that the simulation results are close to the experimental results and that the simulation results have high reliability and practical reference value. Through the above calculation and analysis, we find that the CFD method can well simulate the resistance of the ROV to underwater motion.

Table 6. Comparison of calculated and experimental forces of ROV

| Motion description	Velocity m/s	0.2	0.4	0.6	0.8	1.0
Forward	Experiment forces/N	-	-	176	315	491
	Calculation forces/N	37.2	114.4	189.4	328	502.4
	Error/%	-	-	1.79	3.96	2.26
Backward	Experiment forces/N	41	119	171	304	475
	Calculation forces/N	42.4	120.8	177.8	315.4	492.7
	Error/%	3.31	1.49	3.98	3.75	3.73
Left	Experiment forces/N	45	175	381	702	1119
	Calculation forces/N	42.3	170.3	383.1	680.1	1062.8
	Error/%	−6.0	−2.69	0.55	−3.12	−5.02
Right	Experiment forces/N	43	168	383	703	1103
	Calculation forces/N	42.8	171.9	387.2	686.0	1075.3
	Error/%	−0.47	2.32	1.10	−2.41	−2.51
Down	Experiment forces/N	46	181	400	713	1136
	Calculation forces/N	48.2	192.6	433.9	780.1	1213.1
	Error/%	4.78	6.41	8.48	9.41	6.79
Up	Experiment forces/N	41	186	401	696	-
	Calculation forces/N	43.5	191.3	411.6	699.3	1042
	Error/%	5.72	2.77	2.57	0.46	
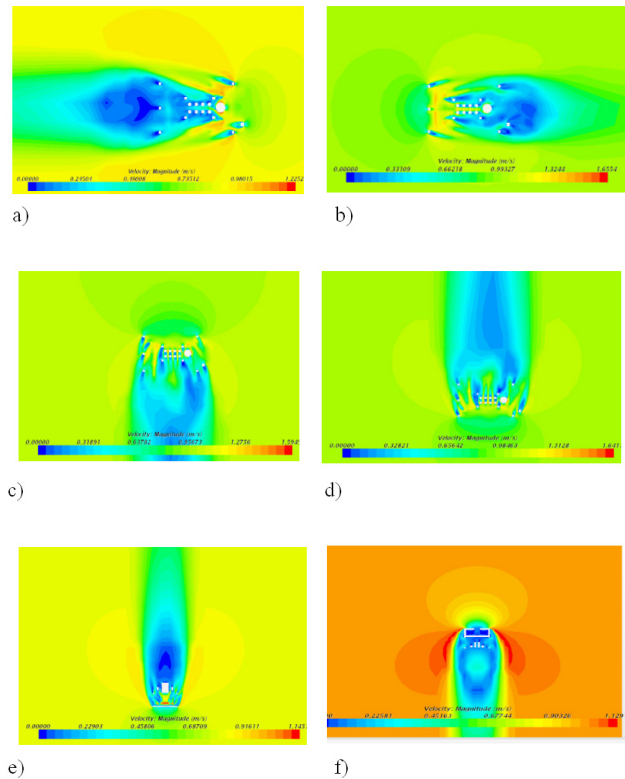
Figure 7. Velocity contours of the ROV different views at a velocity of 1.0 m/s a). the forward view b). the backward view c). the right view d). the left view e). the down view f). the up view

Figure 7 presents the velocity contours of the design velocity of 1.0 m/s and different directions of motion.

A large low-speed zone is formed at the downstream of the ROV, which is also the main generating zone of the vortex. Therefore, a large sticking resistance is generated during the advancement process. In addition to the ROV's own frame, a large part of this low-speed area comes from the ROV. Each small part forms a low-speed area behind it. All components are densely distributed and have a large impact on the flow field. In terms of drag reduction, the water flow should pass through the interior of the ROV as smoothly as possible.
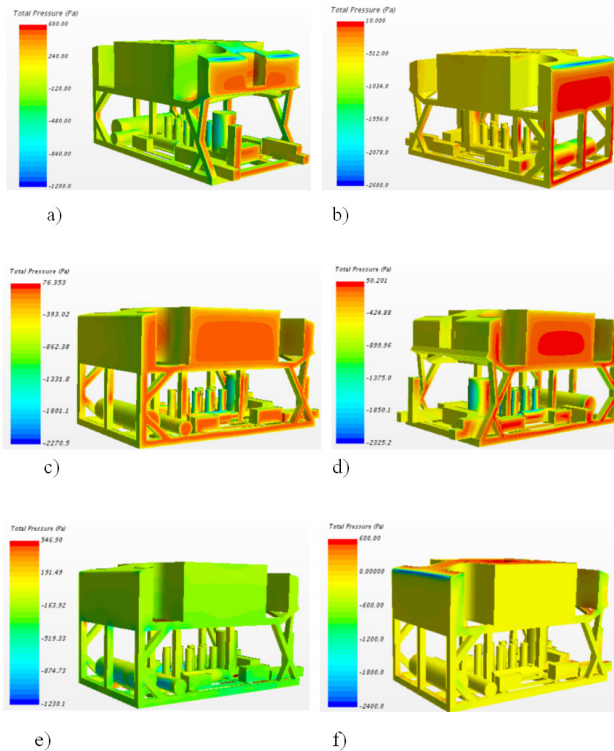

Figure 8. Total pressure contours of the ROV different views at a velocity of 1.0 m/s a). the forward view b). the backward view c). the right view d). the left view e). the down view f). the up view

Figure 8 shows a graph of the ROV's total pressure distribution with different motion patterns at a speed of 1.0 m/s. As a result of the upstream movement of the ROV, the front surface of the ROV is subjected to a large total fluid pressure (red color in the figure), and the total pressures in other areas are small and evenly distributed. The ROV's movement resistance is mainly related to its incident flow area and speed. When the velocity is constant in the incident flow area, the greater the ROV is, the greater the resistance will be.

5.2 Simplified Model Analysis

The actual ROV structure is considerably complicated and is thus not conducive to the numerical simulation of CFD. Therefore, several small components can be simplified into regular geometries without changing the actual flow state inside the ROV. We simplify two main types of geometric components, namely, a cuboid and a cylinder. The effects of the different shape geometries inside the ROV on the resistance performance are studied separately. The original model of the ROV is simplified in three ways. As shown in Figure 9, Case 1 removes all the cuboid members in the ROV and retains all cylindrical members. Case 2 removes all the cylindrical members in the ROV and retains all the cuboid members. Case 3 removes all the cuboids and cylindrical members.
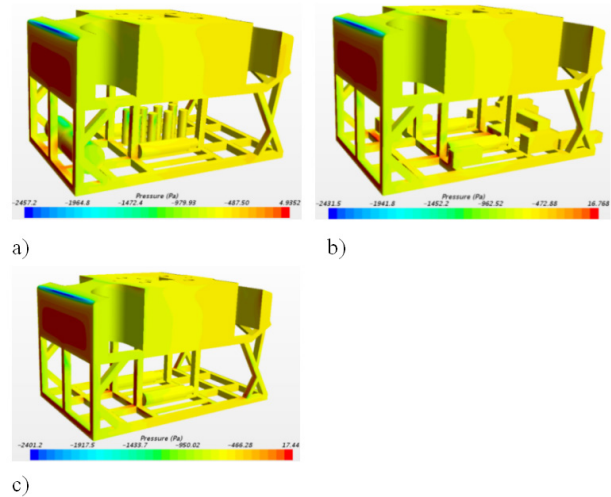
Figure 9. Three Simplified models schemes a). Case1 b). Case 2 c). Case 3
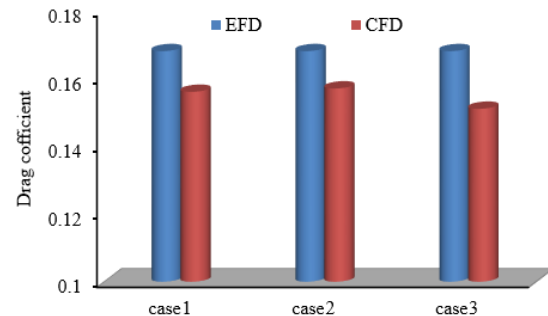
Figure 10. Calculation results of three schemes

Figure 10 presents a comparison of the calculated results of the three simplified models with the experimental values. The navigational resistance calculated by the three simplified schemes is smaller than that of the original model of the ROV. However, the difference between the calculation results and the data of the parent type of the three schemes is not considerably large, especially when all the components of the ROV are removed. Therefore, a simplified model can be used in the

resistance analysis to reduce the computation time.

5.3 Resistance Analysis of Models with Different Lengths and Heights

The principal scale of the ROV affects its resistance performance. In this work, the influence of the change of the principal scale on the resistance of the ROV is studied by changing the length (width and height are unchanged) and height (length and width are unchanged) of the ROV. The empirical formulas for calculating the ROV's navigation resistance varying with the principal scale are fitted. Table 7 shows the variation parameters of the ROV's principal scale. Table 7 presents the model obtained by reducing and enlarging Case 3 in Figure 9 in the longitudinal direction (width and height are unchanged) and height (length and width are unchanged) of the ROV. We analyze its resistance during horizontal navigation. As presented in Table 7, the navigational resistance gradually decreases with the increase of length and the decrease of height.

Table 7. Changes of the length, breadth, and height of the ROV

L	0.7L	0.8L	0.9L	1.0L	1.1L	1.2L	1.3L
Drag coefficient	0.207	0.172	0.155	0.142	0.129	0.119	0.118
B	0.7B	0.8B	0.9B	1.0B	1.1B	1.2B	B1.3
Drag coefficient	0.119	0.127	0.138	0.142	0.154	0.165	0.171
H	0.7H	0.8H	0.9H	1.0H	1.1H	1.2H	1.3H
Drag coefficient	0.132	0.133	0.134	0.142	0.149	0.151	0.152

The empirical formula for calculating the ROV drag coefficient fitted by MATLAB software based on Table 7 is shown in Equation (16). Figure 11 presents the formula fitting diagram.

According to this formula, any type of ROV is suitable for estimating the hydrodynamic performance at the preliminary design stage as long as the principal dimensions (length, width, and height) can be a preliminary estimate of the ROV's motion resistance.

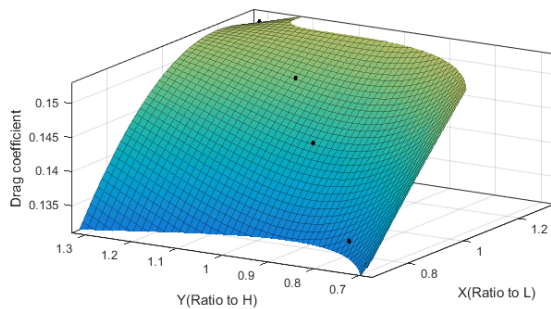$$C_D = 0.04939 - 0.102\sin(-0.3137\pi XY) + 0.1608\exp(-(1.752\,Y)^2) \quad (16)$$

Figure 11. Formula Fitting Diagram

5.4 Resistance Analysis of ROV's Oblique Navigation on the Horizontal Plane

The Re values are $1.27E^{-6}$, $1.59E^{-6}$, and $1.72E^{-6}$. The course angles are $-8°$, $+8°$, $-16°$, $+16°$, $-45°$, $+45°$, $-75°$, and $+75°$. The force and moment of the ROV's oblique navigation on the horizontal plane are calculated by the CFD software star-ccm+. Figures 12 a), b), c), and d) respectively present the surge force, sway force, heave force, and pitching moment of the ROV's oblique navigation on the horizontal plane. As shown in Figure 12a), when the ROV level is tilted, the surge force increases as the speed increases. At the same speed, the smaller the drift angle is, the greater the longitudinal resistance will be. When the drift angle is between $+15°$ and $+45°$ or between $-15°$ and $-45°$, the surge force does not change much, thereby indicating that the transverse current has little effect on the ROV. This result is explained as follows. As the ROV is an open-frame type, the parts of its body are arranged irregularly. Therefore, when a large drift angle occurs, the area behind the flow does not change much. When the drift angle exceeds $45°$, the surge force sharply decreases. As the surge force is decomposed to the transverse direction when the drift angle becomes large, the sway force becomes large.

Figure 12. Forces and moment of the ROV's oblique navigation on the horizontal plane under different Reynolds numbers a). surge force b). sway force c). heave force d). pitching moment

Figure 12b) shows that the sway force of the ROV oblique navigation on the horizontal plane is relatively large and that the sway force increases with speed. At the same speed, the sway force increases as the drift angle increases. When the drift angle increases, the surge resistance is reduced. Thus, special attention should be paid to the influence of transverse currents on the main

heading when the ROV is performing underwater oblique navigation.

Figures 12c)-12d) indicate that the heave force of the ROV's oblique navigation on the horizontal plane is small and that the heave force increases with speed. At the same speed, the heave force decreases as the drift angle increases. The downward pitching moment increases with speed. At the same speed, it increases as the drift angle increases, and the upward pitching moment is considerably small.

a) 8° drift angle   b) 16° drift angle

c) 45° drift angle   d) 75° drift angle
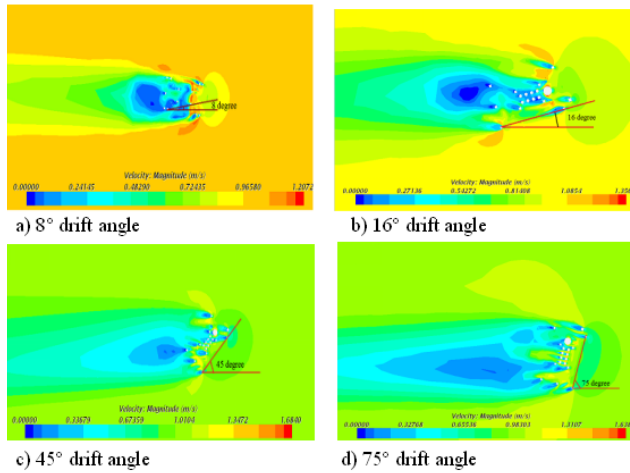
Figure 13. Velocity contours at different drift angles of ROV's oblique navigation on the horizontal plane

Figure 13 shows the velocity contours of a 0.5 m section at different drift angles of the ROV's oblique navigation on the horizontal plane. As the drift angle increases, the low-pressure region of the ROV attachment also becomes large. The presence of the low-pressure region affects the motion stability and equipment performance of the ROV, especially for deep water operations.

5.5 Resistance Analysis of ROV's Oblique Navigation on the Vertical Plane

The Re values are $1.27E^{-6}$, $1.59E^{6}$, and $1.72E^{-6}$. The course angles are −8°, +8°, −16°, +16°, −45°, +45°, −75°, and +75°. The force of the ROV is calculated with the CFD software star-ccm+. As a result of the asymmetry of the upper and lower structures of the ROV, the oblique navigation on the vertical plane calculates the drift angle from negative (water flow from above) to positive (water flow enters from the bottom). Figures 14 a), b), c), and d) are the surge force, sway force, heave force, and pitching moment of the ROV's oblique navigation on the vertical plane, respectively. As the speed increases, the surge force becomes significantly large. At the same speed, the surge

force, the sway force, and the heave force (the upward and downward flow areas of the ROV are different) all increase as the drift angle increases. The sway force and the heave force increase as the speed increases. The pitching moment increases as the speed and as drift angle increase at the same speed. The numerical simulation of the ROV's oblique navigation on the vertical plane can provide an operational basis for cleaning operations.

a)   b)

c)   d)
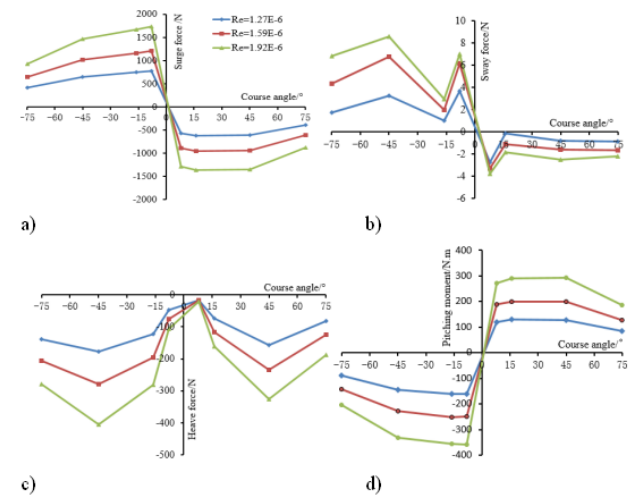
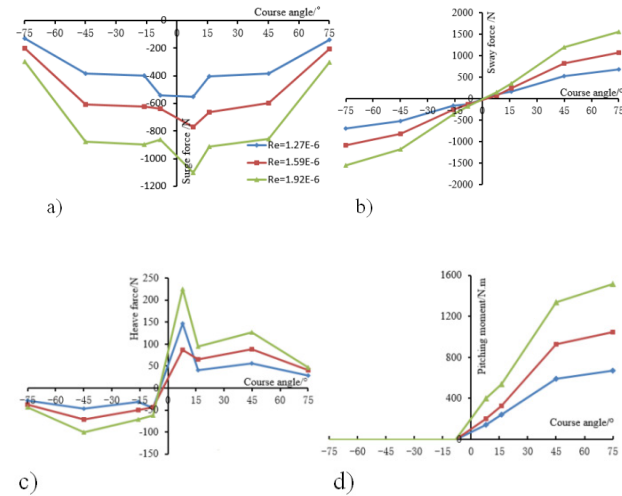**Figure 14.** Forces and moment of ROV's oblique navigation on the vertical plane under different Reynolds numbers a). surge force b). sway force c). heave force d). pitching moment

a) 8° drift angle   b) 16° drift angle

c) 45° drift angle   d) 75° drift angle
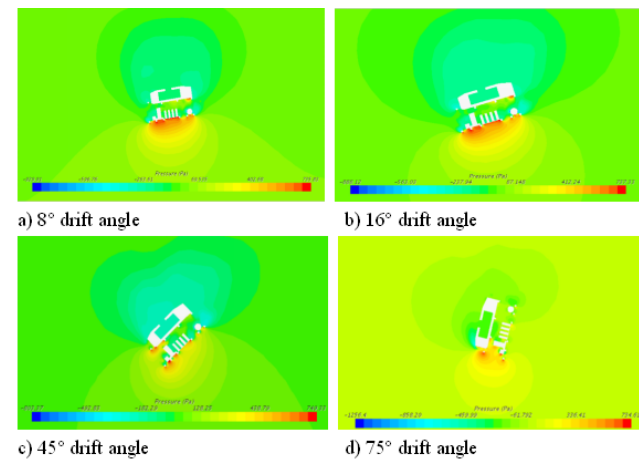
Figure 15. Velocity contours at different drift angles of the ROV's oblique navigation on the vertical plane

Figure 15 shows the velocity contours of the 0.5 m section at different drift angles of the ROV's oblique navigation on the vertical plane. As the drift angle increases, the upward movement speed of the ROV gradually becomes small. Therefore, the change of the drift angle affects the speed and direction of the ROV's movement, especially during deep water operations.

6. Movement Analysis

From the dimensional analysis and by using the Buckingham π theorem, we define the drag coefficient in Equation (17).

$$C_D = \frac{F}{0.5\rho SU^2} \qquad (17)$$

where C_D is the drag coefficient, F is the drag force of the ROV, S is the frontal area of the ROV, U is the velocity of the ROV, and ρ is the fluid density.

Taking the ROV with horizontal motion as a case, we study the motion response of the drag coefficient in 6DOF (yaw, pitch and roll surge, sway, and heave). The drag coefficient for the ROV is a function of the Reynolds number. Thus, the similitude is satisfied by having the same Reynolds number for the two flows. The CFD study for the operating range of flow speeds (0.2 m/s ~ 1.2 m/s) shows that the drag coefficients are nearly constant for the corresponding range of Reynolds number (Figure 16).

The ROV has the largest drag in the heave direction due to its largest frontal area normal to the flow direction of about 1.49 m². The drag force in sway is slightly larger than the drag in the surge direction due to the ROV's small frontal area. The three rotation motions, namely, yaw, pitch, and roll, are plotted against the Reynolds number in Figure 16. As observed from the plots, the ROV has the largest drag in the roll direction due to its largest mass moments of inertia. The drag force in pitch is slightly larger than the drag in the yaw direction due to the ROV's small mass moments of inertia.
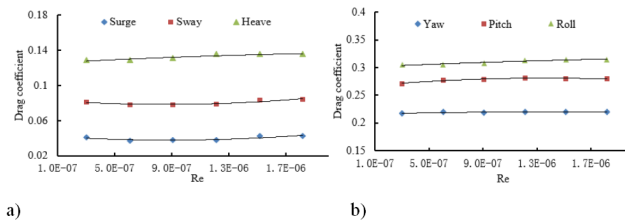

Figure 16. Drag coefficient versus Reynolds number. a). drag coefficient of surge, sway, heave motion b). drag coefficient of yaw, pitch, roll motion

7. Conclusions

The CFD method is used to study the resistance performance and motion stability of an open-frame ROV. The forward, backward, transverse, floating, and submerged resistance of the ROV are simulated and compared with existing experimental values to verify the accuracy of the calculation method. Then, the resistance performance of the ROV's oblique navigation on the horizontal and vertical plane is studied, along with its heave, pitch, and yaw in direct horizontal navigation.

The research results show that due to the structural asymmetry of the open-frame ROV, the pitching moment, transverse force, and longitudinal force are large in the direct horizontal navigation, horizontal oblique navigation, and vertical oblique navigation, respectively. Therefore, the influence of transverse current on the ROV's motion stability should be noted in a specific ROV operation. The simulation results in this work can provide technical support for the resistance prediction and design of deep sea ROVs.

Index of Abbreviations

ROV	remotely operated vehicle
CFD	computational fluid dynamics
PMM	plane motion mechanism
6DOF	six-degree-of-freedom
LabVIEW	Laboratory Virtual instrument Engineering Workbench
RANS	Reynolds-averaged Navier-Stokes
ITTC	International Towing Tank Conference
SIMPLE	Semi-Implicit Method for Pressure Linked Equations

References

[1] Zhang, Y., Xu, G.H., Xu, X.L., et al., 2010. Mensuration of the Hydrodynamic Coefficients of the Micro Miniature Open-shelf Underwater Vehicle. Shipbuilding of China. 51(1), 63-72.

[2] Juan, P., Julca, A., Julio, C.A., 2011. Experimental Evaluation of the Hydrodynamic Coefficient of a ROV Through Morison's Equation. Ocean Engineering. 38(17-18), 2162-2170.

[3] Fan, S.B., Lian, L., 2012. Oblique Towing Test and Maneuver Simulation at Low Speed and Large Drift Angle for Deep Sea Open-Framed Remotely Operated Vehicle. Journal of Hydrodynamics. 24(2), 280-286.

[4] Leong, Z., Ranmuthugala, D., Forrest, A., et al., 2015. Numerical investigation of the hydrodynamic interaction between two underwater bodies in relative motion. Appl Ocean Res. 51, 14-24.

[5] Kang, T., Hu, K., Hu, Z.Q., et al., 2005. Research on maneuverability simulation calculation of underwater vehicle by CFX and USAERO. Robot. 27(6), 535-538.

[6] Alexander, P., Maaten, F., Stephen, R.T., 18-21 June 2007. The use of computational fluid dynamics to assess the hull resistance of concept autonomous underwater vehicles. In: Proceedings of the oceans 2007—Europe, Aberdeen, New York: IEEE. pp.

1292-1297.

[7] Zhang, H., Xu, Y.R., Cai, H.P., 2010. Using CFD software to calculate hydrodynamic coefficient. Journal of Marine Science and Application. 9(2), 149-155.

[8] Wang, T., Ye, X.F., Wang, L., et al., 7-10 August 2011. Hydrodynamic analysis and optimization for dish shaped underwater robot. In: Proceedings of the 2011 international conference on mechanics and automation, Beijing, China. New York: IEEE. pp.1406-1411.

[9] Chin, C., Lau, M., 2012. Modeling and testing of hydrodynamic damping model for a complex-shaped remotely-operated vehicle for control. J Mar Sci Appl. 11(2), 150-163.

[10] Nedelcu, A., Trbu, O., Clinci, C., Ichimoaiei, G., 2018. CFD approach used for modelling hydrodynamic analysis and motion characteristics of a remotely operated vehicle. IOP C Ser Earth Env. 170, 012029.

[11] Badawy, A.M., Omer, A.A., 2013. Dynamic analysis of remotely operated underwater vehicle model. International Journal of Engineering Science Invention. 2(7), 5-16.

[12] José, B.M., Lucas, A.B., 2015. Drag evaluation of a remotely operated vehicle. 23rd ABCM International Congress of Mechanical Engineering, December 6-11, Rio de Janeiro, RJ, Brazil.

[13] Wang, C., Zhang, F., Schaefer, D., 2014. Dynamic modeling of an autonomous underwater vehicle. J Mar Sci Technol. 20(2), 199-212.

[14] Skorpa, S., 2002. Numerical simulation of flow around remotely operated vehicle (ROV). Master's Thesis, Norwegian University of Science and Technology, Trondheim.

[15] Vaz, G., Toxopeus, S., Holmes, S., 6-11 June 2010. Calculation of manoeuvring forces on submarines using two viscous-flow solvers. In: Proceedings of the ASME 2010 29th international conference on ocean, offshore and arctic engineering (Paper no. OMAE2010-20373), Shanghai, China. New York: American Society of Mechanical Engineers. pp. 621-633.

[16] Yu, G., Wang, Z., Ling, H., 2018. Research on hydrodynamic performance of rotatable cable underwater robot. Int J Eng Appl Sci. 5(10), 36-42.

[17] Chin, C.S., Lin, W.P., Lin, J.Y., 2018. Experimental validation ofopen-frame ROV model for virtual reality simulation and control. J Mar Sci Technol. 23(2), 267-287.

[18] Andra, T.N., Catalin, F., Mihail, L.D., 2018. CFD analysis for a remotely operated vehicle in horizontal plan. Mechanical Testing and Diagnosis. 1, 5-10.

[19] Teague, J., Michael Allen, J., Tom, B., 2018. The potential of low-cost ROV for use in deep-sea mineral, ore prospecting. Ocean Eng Monitor. 147, 333-339.

[20] Juan, A., Ram´ırez-Mac´ıas, Persijn, B., et al., 2016. Hydrodynamic modeling for the remotely operated vehicle Visor3 using CFD. Preprints, 10th IFAC Conference on Control Applications in Marine Systems September 13-16, Trondheim, Norway.

[21] Christian, B., Jose, R., Carlos, P.A., 2013. Hydrodynamic Assessment of a Remotely Operated Underwater Vehicle Based on Computational Fluid Dynamic-Part 1-Numerical Simulation. CMES. 90(2), 165-177.

[22] Hung, D.N., Sachith, M., Dev, R., 2013. Design, modeling and simulation of a remotely operated vehicle-part1.Journal of Computer Science and Cybernetics. 29(4), 299-312.

[23] Lau, W., Low, E., Seet, G., et al., 2008. Estimation of the Hydrodynamics Coefficients of an ROV using Free Decay Pendulum Motion. Engineering Letters. 16(3), 326-331.

[24] Muljowidodo, K., Sapto, A.N., Nico, P., et al., 2009. Design and testing of underwater thruster for SHRIMR ROV-ITB. Indian journal of Marine Sciences. 38(3), 338-345.

[25] James, J., Brian, P., 2014. Development of an adaptable monitoring package for marine renewable energy projects part II: hydrodynamic performance. Proceedings of the 2nd Marine Energy Technology Symposium, April 15-18, Seattle, WA.

[26] Mingyu, K., Olgun, H., Osman, T., 2017. Numerical studies on added resistance and motions of KVLCC2 in head seas for various ship speeds. Ocean Eng. 140, 466-476.

[27] Yavuz, H., Ozdemir, B.B., 2017. Numerical study of ship motions and added resistance in regular incident waves of KVLCC2 model. Int J Nav Arch Ocean. 9, 149-159.

[28] Longo, J., Stern, F., 2005. Uncertainty assessment for towing tank tests with example for surface combatant DTMB model 5415. J Ship Res 49(1), 55-68.

[29] Bradshaw, P., Huang, G.P., 1995. The Law of the Wall in Turbulent Flow . Proceedings: Mathematical and Physical Sciences. Osborne Reynolds Centenary. 451(1941), 165-188.

[30] Yang, C., Zhu, R., Miao, G., 2012. Uncertainty Analysis in CFD for Flow Simulation Around Ship Using RANS and DES. Journal of Shang Hai Jiao Tong University. 46(3), 430-435.

ARTICLE

Analysis of Shoreline Changes in Ikoli River in Niger Delta Region Yenagoa, Bayelsa State Using Digital Shoreline Analysis System (DSAS)

Egai Ayibawari Obiene[1*]   Eteh Desmond Rowland[1]   Inko-Tariah Ibiso Michael[2]

1. Department of Geology, Niger Delta University, Wilberforce Island, Bayelsa State, Nigeria
2. Department of Geography and Environmental Management, Rivers State University, Rivers State, Nigeria

ABSTRACT

The use of Digital Shoreline Analysis System was used to determine shoreline changes in Ikoli River, Yenagoa, Bayelsa State. Shoreline data were extracted from satellite imagery over thirty years (1991-2021). The basis of this study is to use Digital Shoreline Analysis System to determine erosion and accretion areas. The result reveals that the average erosion rate in the study area is 1.16 m/year and the accretion rate is 1.62 m/year along the Ikoli River in Ogbogoro Community in Yenagoa, Bayelsa State. The mean shoreline length is 5.24 km with a baseline length of 5.2 km and the area is classified into four zones to delineate properly area of erosion and accretion based on the five class of Linear regression rate, endpoint rate and weighted linear rate of which zone I contain very high erosion and high erosion with an area of landmass 255449.93 m^2 of 38%, zone II contain moderate accretion, very high accretion and high accretion with a land area of 1666816.46 m^2 with 24%, zone III has very high erosion and high erosion with an area of landmass 241610.85 m^2 of 34 % and zone IV contain moderate accretion and high accretion with land area 30888.08 m^2 with 4%. Out of the four zones, zone I and II were found to be eroding with 72% and zone II and IV contain accretion with 28%. The result shows that 44% of the area have been eroded. Therefore, coastal engineers, planners, and shoreline zone management authorities can use DSAS to create more appropriate management plans and regulations for coastal zones and other coastal parts of the state with similar geographic features.

1. Introduction

The shoreline changes have been a major issue in Yenagoa and other parts of the world, resulting in the loss of life and property, including farmlands. The fundamental aspect in the detection of shoreline changes is erosion, accretion and morphodynamics, which is a

---

*Corresponding Author:
Egai Ayibawari Obiene,
Department of Geology, Niger Delta University, Wilberforce Island, Bayelsa State, Nigeria;
Email: desmondeteh@gmail.com

necessity for shoreline computation [1]. Shorelines are the land-sea interface that shifts unpredictably in reaction to one or more causes in nature, such as morphological, climatic, or geological factors [2]. Because of their dynamic environmental setting, shorelines as a borderline between land and sea are subject to constant change [3]. The dynamic interactions between and among waves, tides, rivers, and physical processes determine the shoreline features [4]. Erosion makes the shoreline more vulnerable, which can be dangerous for human activity near the shore. Furthermore, the frequent occurrence of shore disasters makes the shore extremely prone to changes such as floods, illegal sand mining, and boat movement, among other things. It is one of the most dynamic landform types on earth, undergoing fast change as a result of geology, geomorphology, and wave action along the shoreline, as well as recurrent storms, sea-level rise, sediment transport by longshore currents, and anthropogenic activity [5]. Because of its remotely sensed and repeated coverage, high resolution, multispectral capabilities, and cost-effectiveness compared to conventional techniques, remote sensing data have been widely used in shoreline change studies in recent years [6]. Several studies on shoreline change have been undertaken in India using remote sensing and Geographic Information System (GIS) techniques at various periods in the recent past [7,8]. The End Point Rate (EPR) technique, when integrated with satellite images, provides a precise and dependable approach for calculating and analyzing shoreline development [9]. Shoreline change studies can be done in a variety of ways, but the Linear Regression Rate (LRR) provides the ability to employ more than two shorelines [10]. A time series of different shoreline positions are utilized to calculate the rate of shoreline change statistics using the Digital Shoreline Analysis System (DSAS) extension tool. A proper assessment, as well as adequate care, must be taken to assure the accuracy of digitisation. For predicting patterns of shoreline behaviour, the DSAS derivation of the historical rate of change trends as an indicator of future trends has been utilized, assuming continuity in the physical, natural, or anthropogenic forcing that has induced the historical change observed at the location [11]. In this study, the DSAS tool is used to accomplish the following objectives: extracting shorelines from satellite images, analyzing the rate of change in the shoreline over thirty years, and determining the estimated erosion and accretion area.

2. Materials and Method

2.1 Location of Study

The research region is located in the central Niger Delta sedimentary basin of Southern Nigeria (Figure 1), in the Yenagoa Local Government area, which is also the capital of Bayelsa State. The location is located between $4^0 55'0''$ N and $4^0 57'0''$ N, and $6^0 14'30''$ E and $6^0 16'0''$ 25'E longitudes. The area features an excellent road network that connects the study area.
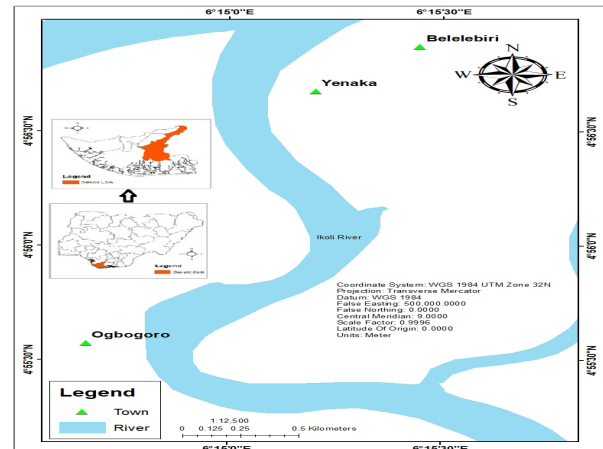
Figure 1. Map of the study area

2.2 Material

Measurement Table, GPS, Geotag Camera, Field noted book and Pen.

2.2.1 Source of Data

The Ikoli River's long-term shoreline change assessment was evaluated for 30 years, from 1991 to 2021. Evaluations of three shorelines extracted from different time-period satellite imageries are used to assess shoreline change. In Table 1, multi-temporal Landsat satellite data for 1991, 2016, and 2021 was acquired from the USGS website [12]. It is better to use satellite data in December or January to prevent mist and haze, as well as other types of atmospheric problems. As a result, satellite data for December and January of each study year was retrieved.

Table 1. List of Data Satellite collected

Satellite Data	Date	Spatial Resolution (m)	Source
Landsat 5	28/02/1991 Path: 189, Row: 57	30	[12]
Landsat 8	26/12/2016 Path: 189, Row: 56	30	[12]
Landsat 8	6/1/2021 Path: 189, Row: 56	30	[12]
Google Earth Imagery	06/02/2021	3m	[12]

2.2.2 Data Processing

Shorelines from multi-temporal satellites are retrieved in vector data form using online visual digitizing in ArcGIS10.6. For shoreline extraction, each multi-temporal satellite image was manually scanned and individually digitized. After that, the shoreline data from various periods were entered into the Digital Shoreline Analysis System (DSAS) for further computation of shoreline change over 30 years from 1991 to 2021 (Figure 2). The ObjectID (a unique number provided to each item), shape (polygon), date (original year), and shape length, ID, and uncertainty values are all used in the DSAS program to generate shoreline positions. In the attribute table, shorelines extracted at different dates were merged as a single feature, resulting in a single shapefile including numerous shorelines. The cross-shore transacts for calculating the shoreline change are collected and generated by meticulously digitizing the direction and shape of the outer shoreline baseline. The rates of shoreline change were calculated using the United States Geological Survey's ArcGIS tool and the DSAS version 5 software (USGS).

2.3 Methods

2.3.1 Statistical Technique

Statistical techniques like Linear Regression Rate (LRR), End Point Rate (EPR) and Net Shoreline Movement (NSM) in DSAS were used in the study.

DSAS version 5.0 tool developed by the USGS is an extension for ArcGIS version 10.6 software. It uses several statistical techniques to compare shoreline positions through time and evaluate shoreline changes the methods used in DSAS are described below and other statistical parameters are described by Himmelstoss et al.[13].

2.3.2 Long-term Changes

Long-term shoreline changes are calculated using multi-temporal Landsat satellite data. We employed a linear regression rate of change statistics after digitizing multi-temporal satellite data, which is determined by fitting a least square regression line to all shoreline points for certain transacts. Then, in the Weighted Linear Regression (WLR) approach, a weight value was added, which represents the uncertainty associated with each shoreline. According to Genz et al.[14], the weight (w) is defined as a function of the variance in the uncertainty of the measurement (e).

$$W = 1(e)^2 \qquad (1)$$

2.3.3 Uncertainties and Errors

Total Positional Uncertainty (Et) is the result of all errors that were previously estimated. It is defined as the square root of the sum of the squares of the sources of previous errors[15]. It was calculated by using (2):

$$Et = \pm \sqrt{E^2s + E^2td + E^2d + E^2p + E^2r} \qquad (2)$$

where Es is the seasonal error, Et is the tidal error, Ed is the digitizing error, Ep is the pixel error, and Er is the rectification error. The total positional uncertainties were used as weights (weighted linear regression or weighted least squares) in the shoreline change analysis in the DSAS.

2.3.4 Net Shoreline Movement (NSM)

NSM is associated with the dates of two shorelines. It reports a distance in meters. It calculates the distance between the oldest and the youngest shorelines at each transect[11].

2.3.5 Shoreline Change Envelope (SCE)

SCE calculates a distance in meters between "the shoreline farthest from and closest to the baseline at each transect"[13]. It is not associated with the dates of these shorelines[13].

2.3.6 End Point Rate (EPR)

EPR is determined by dividing NSM by the period elapsed, as in (3)[16,13,11].

$$R = D/T_e \qquad (3)$$

where R is in meters per year (m/yr), D is in meters and T_e is the period elapsed between the oldest and the most recent shoreline (years). EPR still works well when we have only two shorelines to analyze the evolution[17].

2.3.7 Linear Regression Rate (LRR)

LRR corresponds to the value of the slope of a least-squares regression line, as in (4), that fits all points of intersection between all shorelines and a specific transect[11,18].

$$y = m.x + b \qquad (4)$$

where y is the distance from baseline, m is the slope (LRR method), and b is the y-intersect (where the line crosses the y-axis)[13].

2.3.8 Weighted Linear Regression rate (WLR)

The WLR approach determines the best-fit regression line by using linear regression with a weight (for each coastline

position) based on the shoreline uncertainty. The weight is the squared total positional uncertainty reversed [15].

This method increases the influence of shoreline points with smaller total positional uncertainty on the best-fit regression line. The slope of this regression line is the shoreline change rate in m/yr, as in (5).

$$y = m_w.x + b_w \qquad (5)$$

where m_w is the slope (WLR method) and b_w is y-intersect [13]. WLR method requires at least three historical shoreline positions [15].

3. Results and Discussion

3.1 Extraction of the Shorelines from the Satellite Imageries

The shoreline changes along with various towns and their environs, as seen in Figure 2 is extracted from Landsat imagery using ArcGIS software. In 1991 the extracted shoreline length is 4.87 km, 2016 is 5.66 km and 2021 is 5.20 km and the shoreline changes from 1991 to 2016 is 25years and 1991 to 2021 is 30 years which make it to be long term changes which as a result led to destroy of building and farmland due to erosion activities in the area in Figure 3 and it means shoreline length is 5.24 km while the baseline length is 5.2 km.
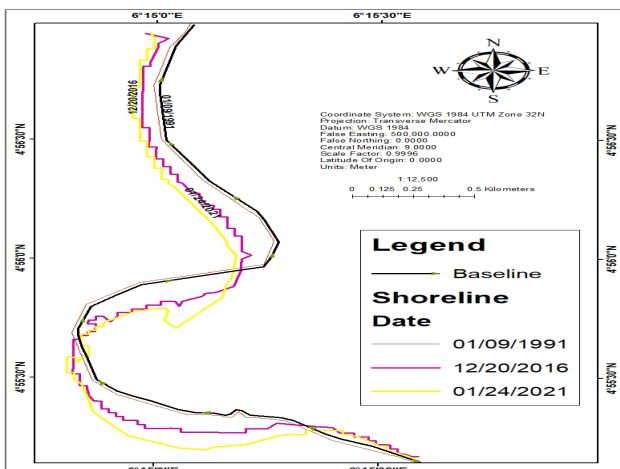

Figure 2. Map showing shoreline changes in Ikoli River

Table 2. Shoreline length and date from satellite

S/N	Date	Shoreline length (km)	Baseline Length (km)
1	01/09/1991	4.87	
2	12/20/2016	5.66	5.2
3	01/24/2021	5.20	
	Mean	5.24	

Figure 3. Image of erosion activities along Ikoli River in Ogbogoro Town, Yenagoa Bayelsa State in 2021.

3.2 Rate of Shoreline Change in Different Zones

DSAS computed total transacts 196 for the whole Ikoli River and the rate of shoreline changes for four zones in the study area in Table 3 and Figure 4 shows that zone I, has 2.02 km in 1991, 2.26 km in 2016 and in 2021 the shoreline length is 1.81 km in Figure 5 with erosion present and 81 transects numbers identify with transect order ranging from 113 to 193, short count contain 2 as 2 and 3 as 78 with an azimuth of 230.23 minimum and 344.626 maximum, but a majority of the transect shows erosion. The average rate over 153 transects, was −3.91 m/ year along those transects with erosion trend, the overall shoreline change rate shows a negative trend throughout the zone indicating erosion is reported along the shoreline in Ogbogoro community and also from Figure 5 the highest shoreline length zone is found in zone I from 1991

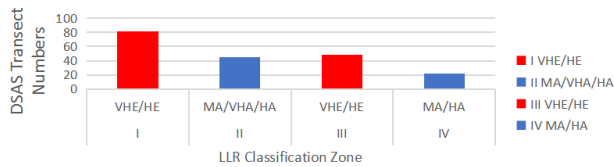to 2016 and 2021 while the lowest shoreline length is identified in zone IV from 1991 to 2016 and 2021.

Figure 4. DSAS Transect Numbers Erosion and Accretion zone

Table 3. DSAS Transect Numbers and Shoreline Length zone

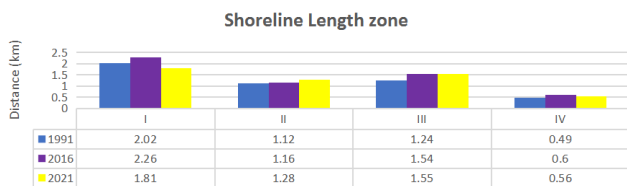| S/N	Zone	DSAS Transect Numbers	shoreline Length (km)		
			1991	2016	2021
1	I	81	2.02	2.26	1.81
2	II	45	1.12	1.16	1.28
3	III	48	1.24	1.54	1.55
4	IV	22	0.49	0.60	0.56

Figure 5. Shoreline Length zone from 1991 to 2021

In zone II, the overall shoreline change rate shows a positive trend throughout the zone, indicating accretion is present along the shoreline. The shoreline change rate contains a shoreline length of 1.12 km in 1991, 1.16 km in 2016, 1.28 km in 2021, and is observed to contain accretion in Table 10 and Figure 9. The average rate over 45 transects was 4.56 m/year along those transects, with transect order ranging from 69 to 113, and short counts contained 2 as 4 and 3 as 43 with an azimuth of 255.57 minimum and 344.46 maximum in Table 10 and the majority of the area increase in land from the flow of water against a shore or bank in Figure 8.

For zone III, the shoreline change analysis shows an erosion trend in Table 11 and Figure 9, but erosion is significant. In this zone, the shoreline change rate contains a shoreline length of 1.24 km in 1991, 1.54 km in 2016, 1.55 km in 2021, and the average erosion is 5.20 m/year. Erosion is observed along the shoreline of the Ikoli river with transect numbers of 48 and a minimum value of azimuth of 129.80 and a maximum value of 257.4.

In zone IV in Table 3 and 12, the average rate over

22 transects was 1.50 m/year along those transects, with a transect order ranging from 1 to 43, with an azimuth of 203.4 min. and 217 max. in Table 12, and the area showing an increase in land from the flow of water against a shore in Figure 8 with a shoreline change rate of 0.49 km in 1991, 0.60 km in 2016, and 0.54 km in 2021.

3.3 Estimation Erosion and Accretion Area

The study area has been classified into four zones in Table 4 and Figure 6, indicating zone I has a 265449.93 m^2 area with very high erosion and high erosion in the study area, with 38% in Figure 5. Zone II contains 166816.46 m^2 with moderate accretion, high accretion, and very high accretion, with 24% in Table 5. Zone III has a 241610.85 m^2 area of landmass with very high erosion and high erosion present, indicating 34% of the mass land is eroded in Table 5, Figures 6 and 8. Zone IV contains 30888.08 m^2 in Tables 4 and 7 with moderate accretion and high accretion present at 4% in the zone.

From Table 6, the result indicates that the percentage of erosion is greater than the percentage of accretion, i.e. the total percentage of erosion is 72% and accretion is 28%, but the percentage difference is 44%. This implies that 309356.20 m^2 of the mass of land in the Ogbogoro community is eroded and the government and relevant agencies like NDDC need to come to their aid to embark on land reclamation and shoreline protection to avoid continued loss of land and properties.

Table 4. Estimate area of Linear regression rate zone

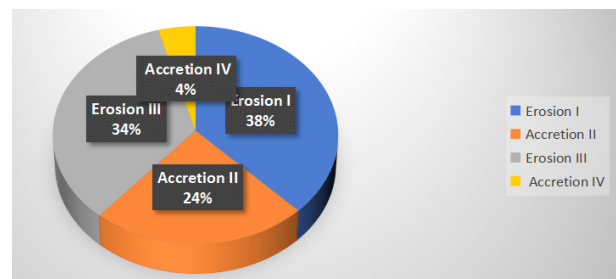| S/N	Zone	Area (m^2)	LRR
1	I	265449.93	VHE/HE
2	II	166816.46	MA/VHA/HA
3	III	241610.85	VHE/HE
4	IV	30888.08	MA/HA

Figure 6. Zone Area in Percentage of Erosion and Accretion

Table 5. Percentage of Erosion and Accretion zone

S/N	Zone	LRR	%
1	I	Erosion	38
2	II	Accretion	24
3	III	Erosion	34
4	IV	Accretion	4

Table 6. Total Percentage of Erosion and Accretion zone

S/N	Zone	LLR	Area (m^2)	Total %
1	I and III	Erosion	507060.8	72
2	II and IV	Accretion	197704.5	28
Difference			309356.3	44
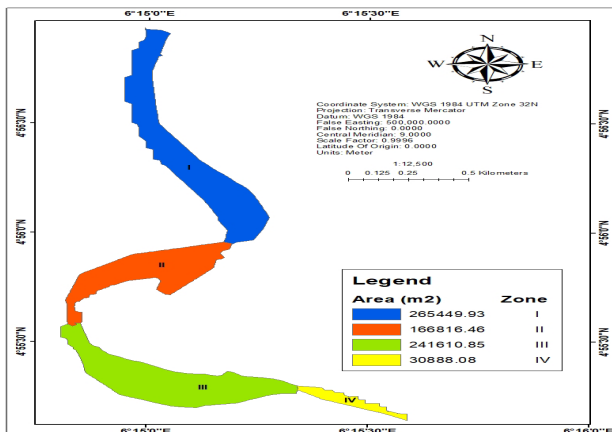
Figure 7. Map showing shoreline Area in Ikoli River
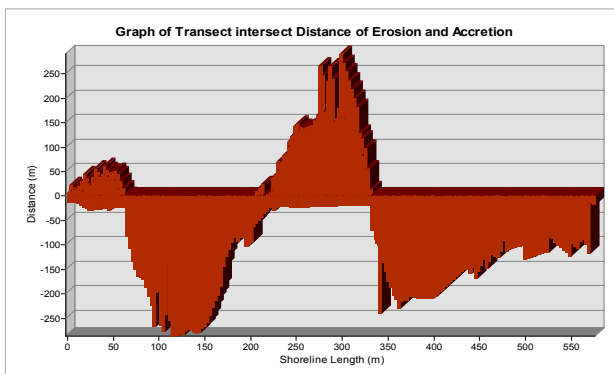
Figure 8. Transect interest Distance of erosion and Accretion

3.4 Mean Shoreline Change Trend in the Selected Zones of Ikoli River

There is a variation in the mean rate of accretion and erosion in the four selected Ikoli River Linear Regression Rate (LRR) which are classified into five, namely very

high erosion, high erosion, moderate accretion, high accretion, and very high accretion in Figure 10 and Table 7. Figure 9 shows that the mean erosion rate of 3.91 m/year is found in zone I, which contains both very high erosion and high erosion. This is the highest compared to zone III, which has a mean of 5.56 m/year and is the lowest in Figure 9, which also contains very high erosion and high erosion in Table 8. The mean annual accretion for zone 2 is 4.56 m/year and is the highest rate that is found along the zone, while zone IV is 1.51 m/year as shown in Figure 9, Table 10, and 12.
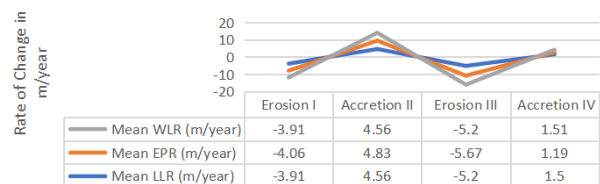
Figure 9. Erosion and Accretion Trend
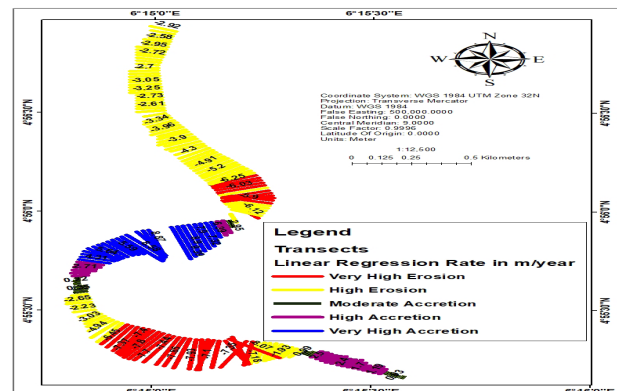
Figure 10. Shoreline accretions and erosion in Ikoli River with LRR

Table 7. Linear regression rate of five classes

S/N	LLR	LRR
1	−8.07- −5.84	Very High Erosion (VHE)
2	−5.84 - −0.52	High Erosion (HE)
3	−0.52 - 1.02	Moderate Accretion (MA)
4	1.02 - 3.82	High Accretion (HA)
5	3.82 - 9.39	Very High Accretion (HA)

Table 8. Linear regression rate zone

S/N	Zone	LRR
1	I	VHE/HE
2	II	MA/VHA/HA
3	III	VHE/HE
4	IV	MA/HA

There is a deviation in the mean rate of accretion and erosion in the four selected Ikoli River in terms of End Point Rate (EPR) in Figure 11. Mean accretion rate of 4.83 m/year is found in zone II which is highest amongst all in Figure 9 and Table 10, whereas zone IV has an accretion rate of 1.19 m/year in Table 12 and Figure 9 while Mean erosion for zone I and III is −4.06 and −5.67 m/year respectively in Figure 9.
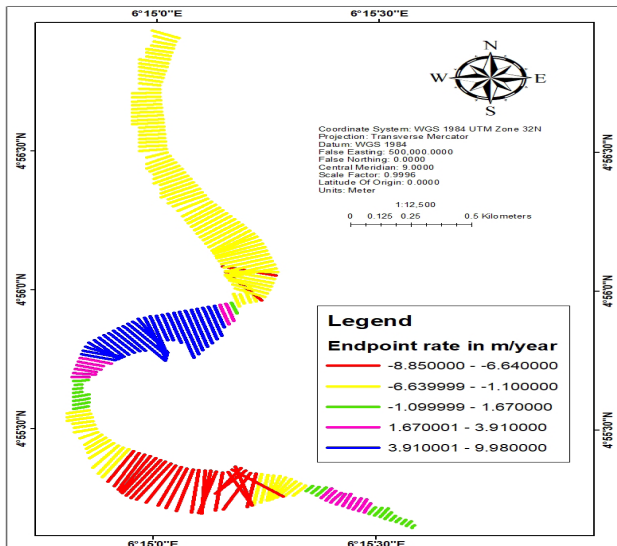

Figure 11. Shoreline accretions and erosion in Ikoli River with EPR

The Weighted Linear regression (WLR) in Figure 12, mean accretion rate of 4.56 m/year is found in zone II which is highest amongst all in Figure 9 and Table 10, whereas zone IV accretion rate 1.52 m/year which is lowest amongst all in Table 12 and Figure 9. Mean erosion for zone I is −0.91 and −5.2 m/year respectively Figure 9.
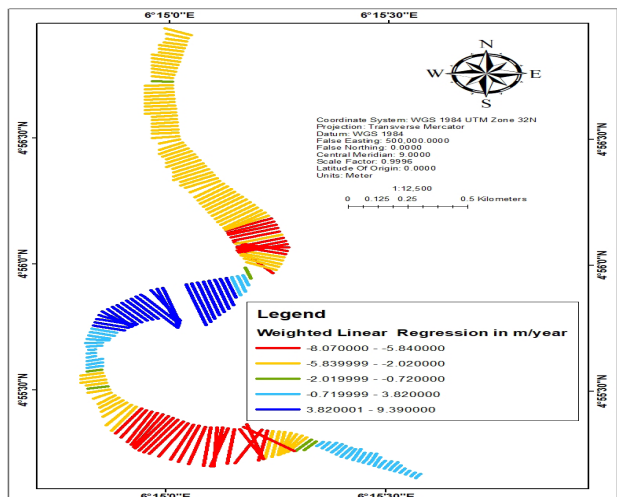

Figure 12. Shoreline accretions and erosion in Ikioli River with WLR

The results from zone I in Table 9 and Figure 13 indicated that the Net Shoreline Movement (NSM) ranged from −219.47 to −43.18 m with a mean shape length of 0.14 km, indicating erosion. Zone II contains a minimum value of 51.88 m and a maximum value of 309.64 m with an average value of 0.15 km, indicating accretion in Table 10. Zone III ranges from −274,83 to −11.33 m and has a mean value of −173.91 with a mean shape length of 0.19 km, indicating erosion in Table 11, and Zone IV has a range value of 17.055 m to 77.35 m with a mean value of 0.05 km, indicating accretion in Table 12.
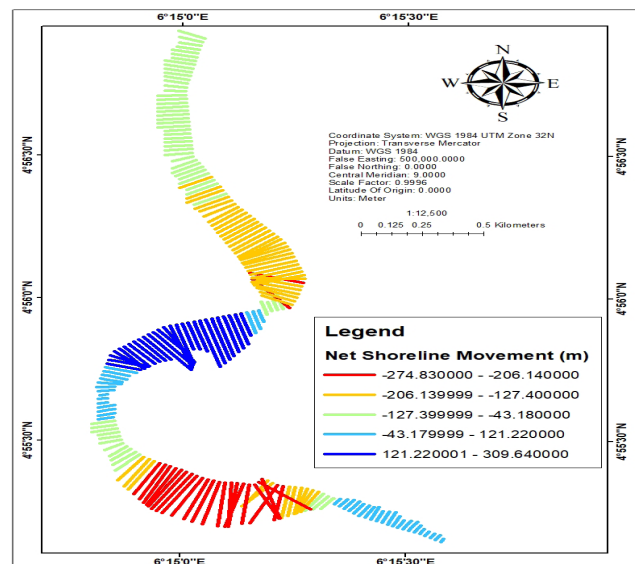

Figure 13. Shoreline accretions and erosion in Ikioli River with NSM

The study was carried out to examine the Ikoli River's shoreline modification. The findings suggest that the majority of the shoreline is at risk of erosion (Table 4 and Figure 14). When erosion and deposit are assessed in the four zones of the research region, erosion dominates while accretion is less active along the shore. The geology, as well as other physical and cultural elements, of the Ikoli River shore region, are diverse. Physical inspection in Figure 8 reveals sand, clay, sand dunes, deltas, and other features. Understanding the mechanisms of erosion, sediment deposition, flooding, and sea-level changes that alter the shoreline is critical for planning shore protection work because erosional processes can affect the stability and productivity of the aquatic environment, which can have serious consequences for the community along the shore. Because of the tidal water pressure, loose bank materials, and shoreline pattern, freshly exposed and steep slope sites are more active in the erosion process. Under the influence of river power, coastline erosion results in the migration of the shoreline onto land and bottom

bed erosion. Disasters in shared areas are caused by both natural and manmade reasons. Wind, waves, tides, sediment supply, changes in relative sea level, and human interventions all affect the shoreline, and these activities constantly generate shoreline changes across a range of time intervals. The above study has consequences for the design and development of the Ogbogoro community's shore tract, as well as other shore locations, in terms of infrastructure development, tourism, and recreational places, among other things. It can also help identify coastal vulnerability in terms of shoreline dynamics and the hazards that come with them.
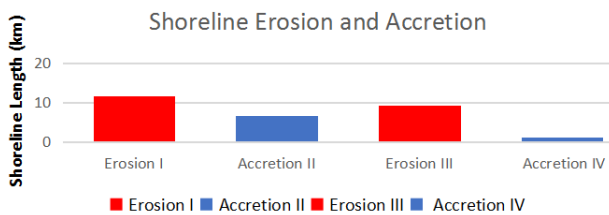

Figure 14. Shoreline Erosion and Accretion

3.6 Risk Analysis of Shoreline Changes

Risk analysis is vital in studying the shoreline for

effective planning and management circumstances in the Niger Delta and other regions of the world to avoid serious erosion consequences. It is also critical to understand the terrain of the area by conducting hydrological and surface assessments to investigate the statuary of the area, particularly in terms of the drainage system, when making decisions for the construction of structures and site suitability, including settlements, farming, road and railway construction. Building structures and piling the shoreline in the study area could have reduced the loss of life because most areas of terrain have poor drainage systems resulting to loss of properties (Figure 3).

4. Conclusions

This study showed that combining remote sensing and GIS technology can be extremely valuable for long-term shoreline change studies using Landsat imagery with reasonable precision. The average erosion rate in the research region is 1.16 meters per year, whereas the accretion rate is 1.62 meters per year along the Ikoli River in Ogbogoro, Bayelsa State. The mean shoreline length is 5.24 km with a baseline length of 5.2 km and the area is classified into four zones to delineate properly area of erosion and accretion based on the five class of Linear

Table 9. Statistical technique results from Digital Shoreline Analysis System Zone 1

	Trans Order	Azimuth	Shr Count	TCD	SCE	NSM	EPR	LRR	WLR	Length (km)
Mini	113.00	230.23	2.00	2825.00	43.18	−219.47	−7.07	−6.39	−6.39	0.06
Max	193.00	344.26	3.00	4825.00	219.47	−43.18	−1.67	−0.90	−0.90	0.24
Mean	153.00	264.36	2.95	3825.00	125.58	−125.19	−4.06	−3.91	−3.91	0.14

Table 10. Statistical technique results from Digital Shoreline Analysis System Zone II

	TransOrder	Azimuth	ShrCount	TCD	SCE	NSM	EPR	LRR	WLR	Length(km)
Mini	69.00	255.57	2.00	1725.00	28.44	51.88	1.67	−0.90	0.90	0.01
Max	113.00	344.46	3.00	2825.00	309.64	309.64	9.98	9.39	9.39	0.31
Mean	91.00	310.92	2.89	2275.00	157.88	145.30	4.83	4.56	4.56	0.15

Table 11. Statistical technique results from Digital Shoreline Analysis System Zone III

	TransOrder	Azimuth	ShrCount	TCD	SCE	NSM	EPR	LRR	WLR	Length (km)
Mini	22.00	129.80	2.00	550.00	41.76	−274.83	−8.85	−8.07	−8.07	0.03
Max	69.00	257.40	3.00	1725.00	274.83	−11.33	−0.37	−0.72	−0.72	0.27
mean	45.50	209.64	2.94	1137.50	176.11	−173.91	−5.67	−5.20	−5.20	0.19

Table 12. Statistical technique results from Digital Shoreline Analysis System Zone IV

	TransOrder	Azimuth	ShrCount	TCD	SCE	NSM	EPR	LRR	WLR	Length(km)
MIN	1.00	203.40	2.00	25.00	20.17	17.05	0.57	0.37	0.37	0.003
MAX	22.00	217.66	3.00	550.00	86.92	77.35	2.49	2.58	2.58	0.09
MEAN	11.50	211.09	2.92	287.50	59.10	36.96	1.19	1.50	1.51	0.05

regression rate, endpoint rate and weighted linear rate of which zone 1 contain very high erosion and high erosion with an area of landmass 255449.93 m^2 of 38%, zone II contain moderate accretion, very high accretion and high accretion with a land area of 1666816.46 m^2 with 24%, zone III has very high erosion and high erosion with an area of landmass 241610.85 m^2 of 34 % and zone IV contain moderate accretion and high accretion with land area 30888.08 m^2 with 4%. Out of four zones, zone I and II are found to be eroding with 72% and zone II and IV contain accretion with 28%. The result shows that 44% of the area has been eroded. Therefore, Coastal engineers, planners, and shoreline zone management authorities may find the map output more useful in developing appropriate management plans and regulations for the beach or coastal zones of the Ikoli River, as well as other coastal areas of the state with similar geographic circumstances.

Recommendations

The rate of change along the shoreline must be monitored to detect eroding areas from time to time.

References

[1] Armenio, E., Serio, F., Mossa, M., Petrillo, A.F., 2019. Coastline evolution based on statistical analysis and modeling. Natural Hazards and Earth System Sciences. 19(9), 1937-1953.
DOI: https://doi.org/10.5194/nhess-19-1937-2019.

[2] Mujabar, P.K., Chandrasekar, N., 2013. Shoreline change analysis along the coast between Kanyakumari and Tuticorin of India using remote sensing and GIS. Arabian Journal of Geosciences. 6, 647-666.
DOI: https://doi.org/10.1007/s12517-011-0394-4.

[3] Mentaschi, L., Vousdoukas, M.I., Pekel, J.F., Voukouvalas, E., Feyen, L., 2018. Global long-term observations of coastal erosion and accretion. Scientific Reports. 8(1), 12876.

[4] Passeri, D.L., Hagen, S.C., Medeiros, S.C., Bilskie, M.V., Alizad, K., Wang, D., 2015. The dynamic effects of sea level rise on low-gradient coastal landscapes: a review. Earth's Future. 3, 159-181.

[5] Zhang, Y., Xie, J., Liu, L., 2011. Investigating sea-level change and its impact on Hong Kong's coastal environment. Annals of GIS. 17(2), 105-112.
DOI: https://doi.org/10.1080/ 19475683.2011.576268.

[6] Lillesand, T.M., Kiefer, R.W., Chipman, J.W., 2015. Remote Sensing and Image Interpretation.

[7] Chandrasekar, N., Viviek, V.J., Saravanan, S., 2013. Coastal vulnerability and shoreline changes for southern tip of india-remote sensing and GIS approach. Journal of Earth Science & Climatic Change. 04(4), 1000144.

DOI: https://doi.org/10.4172/2157- 7617.1000144.

[8] Kaliraj, S., Chandrasekar, N., Magesh, N., 2013. Evaluation of coastal erosion and accretion processes along the south-west coast of Kanyakumari, Tamil Nadu using geospatial techniques. Arabian Journal of Geosciences. 8(1), 239-253.
DOI: https://doi.org/10.1007/s12517-013-1216-7.

[9] Sebat, M., Salloum, J., 2018. Estimate the rate of shoreline change using the statistical analysis technique (Epr). Business & It Viii (1). pp. 59-65.
DOI: https://doi.org/10.14311/bit.2018.01.07.

[10] Burningham, H., French, J., 2017. Understanding coastal change using shoreline trend analysis supported by cluster-based segmentation. Geomorphology. 282, 131-149.
DOI: https://doi.org/10.1016/j.geomorph.2016.12.029.

[11] Oyedotun, T.D.T., 2014. Shoreline Geometry: DSAS as a Tool for Historical Trend Analysis. In Geomorphological Techniques edited by Clarke, L. and Nield, J. M.. British Society for Geomorphology: London,UK. 1-12. ISSN:2047-0371.

[12] https://earthexplorer.usgs.gov/

[13] Himmelstoss, E.A., Henderson, R.E., Kratzmann, M.G., Farris, A.S., 2018. Digital shoreline analysis system (DSAS), version 5.0 user guide. U.S. Geological Survey Open-File Report 2018-1179. 2331-1258 (online). pp. 110.
DOI: https://doi.org/10.3133/ofr20181179

[14] Genz, A., Fletcher, C., Dunn, R., Frazer, L., Rooney, J., 2007. The predictive accuracy of shoreline change rate methods and alongshore beach variation on Maui, Hawaii. Journal of Coastal Research. 231, 87-105.
DOI: https://doi.org/10.2112/05-0521.1.

[15] Fletcher, C.H., Romine, B.M., Genz, A.S., Barbee, M.M., Dyer, M., Anderson, T.R., Lim, S.C., Vitousek, S., Bochicchio, C., Richmond, B.M., 2011. National Assessment of Shoreline Change: Historical Shoreline Changes in the Hawaiian Islands. Washing-ton, DC: U.S. Geological Survey Open-File Report. 2011-1051.

[16] Chand, P., Acharya, P., 2010. Shoreline change and sea level rise along coast of Bhitarkanika wildlife sanctuary, Orissa: an analytical approach of remote sensing and statistical techniques. International Journal of Geomatics and Geosciences. 1, 436-455.

[17] Thieler, E.R., Himmelstoss, E.A., Miller, T., 2005. Digital Shoreline Analysis System (DSAS) version 3.0: An ArcGIS extension for calculating shoreline change. In, Extension for ArcGIS.

[18] Prukpitikul, S., Buakaew, V., Keshdet, W., Kongprom, A., Kaewpoo, N., 2012. Shoreline Change Prediction Model for Coastal Zone Management in Thailand. Journal of Shipping and Ocean Engineering. 2, 238-243.

Journal of Marine Science

https://ojs.bilpublishing.com/index.php/jms

EDITORIAL
Climate Change Effects and Marine Renewable Energy Important Topics Targeted by the *Journal of Marine Science*

Eugen Rusu[1,2*]

1. Editor in Chief, Journal of Marine Science
2. Faculty of Engineering, "Dunărea de Jos" University of Galati, 800201, Galati, Romania

The higher dynamics in the climate change became quite visible in the last decades. Although there are still theories assuming these changes to the cyclic character of the climate, it is obvious that this dynamics is also driven to a large extent by the human activities. According to the Intergovernmental Panel on Climate Change (IPCC), which is the United Nations body for assessing the science related to climate change, various climate scenarios have been designed. Thus, in the framework of the Fifth Assessment Report (AR5) [1], the RCP concept has been introduced. RCP stands for Representative Concentration Pathway and represents the greenhouse gas concentration (not emissions) trajectory adopted by the IPCC. Four pathways were initially used for climate modelling, describing different climate futures, all of which are considered possible depending on the volume of greenhouse gases (GHG) emitted in the years to come. The RCPs - originally RCP2.6, RCP4.5, RCP6, and RCP8.5 - are labelled after the possible range of radiative forcing values in the year 2100 (2.6, 4.5, 6, and 8.5 W/m^2, respectively). Further on, according the Sixth Assessment Report (AR6) [2], the original pathways are considered in the framework of a wider concept, which is the Shared Socioeconomic Pathways (SSPs). Furthermore, new RCPs were also designed, such as RCP1.9, RCP3.4 and RCP7. These SSPs are holistic approaches describing scenarios of projected socioeconomic global changes up to 2100. They are used to derive greenhouse gas emissions scenarios with different climate policies. The new designed scenarios are: SSP1: Sustainability (Taking the Green Road), SSP2: Middle of the Road, SSP3: Regional Rivalry (A Rocky Road), SSP4: Inequality (A Road

*Corresponding Author:
Eugen Rusu,
Editor in Chief, Journal of Marine Science; Faculty of Engineering, "Dunărea de Jos" University of Galati, 800201, Galati, Romania;
Email: eugen.rusu@ugal.ro

divided) and SSP5: Fossil-fueled Development (Taking the Highway). Under these circumstances, it is obvious that decarbonisation should become a high priority, and an important step towards a significant emission reduction is represented by increasing substantially the percentage of the Green Energy in the global energy portfolio.

Marine environment is very sensitive to the climate changes [3] and the effects can be locally much more dramatic even than the most pessimistic climate scenarios [4]. On the other hand, marine areas are very rich in various forms of clean energy that can be extracted. In the first place, ocean energy is very significant for island environments [5,6]. These are in general remote areas where the conventional sources of energy are quite expensive, but where marine renewable energy is abundant [7]. Marine renewable energy can represent also a viable solution for the developing countries [8], as for example those from South America [9] that have extended coast both at Atlantic and Pacific oceans. Furthermore, besides providing clean energy, the marine energy farms can play an active role also in coastal protection [10-15]. Thus, by absorbing the energy of the incoming waves the marine power projects can influence in a significant way the coastal dynamics contributing in reducing the erosion and attenuate many nearshore processes. Thus, the marine projects can act as drivers for the nearshore currents changing the costal circulation and modelling the sediment transport patters.

As regards Europe, this is not only a pioneer in re-lationship with the development of the marine energy projects, but at the same time, is still the world leader in ocean energy extraction. In fact, the first offshore wind farm in the world (Vindeby) was installed in 1991 in the Baltic Sea by Denmark and at this moment this wind project is still operational. Furthermore, the Baltic Sea is among the coastal environments where the offshore wind farms have been systematically implemented in the last decades, with 18 operational wind farms [16]. However, the most significant European marine area, and probably one of the most significant in the world, from the point of view of harnessing the marine energy resources is the North Sea, where around 40 wind projects are nowadays operating [17]. Furthermore, huge projects are planned for this marine area, where an artificially constructed island is planned to be built by Denmark 80 kilometres from the shore of the Jutland peninsula. Thus, around 200 wind turbines with a combined capacity of 3 GW are expected to be installed in the first phase of the project by 2030.

In the global context of following the green path and reducing the CO_2 emissions, European Union developed a coherent and ambitious strategy. From this perspective, in December 2019 the European Green Deal was publically released [18]. This document presents the European strategy for decarbonisation, according to which the European Union is assumed to become climate neutral by 2050. An important step in achieving such ambitious target is represented by a significant enhancement in extracting marine renewable energy. Thus, although the offshore wind industry has had an exponential increase in the last decade, the EU target assumed for 2050 is a 25 times increase than the current operating capacity of 12 GW (in 2021). It is obvious that such target implies both high technological advance and wide geographical extension. From this perspective, besides the traditional areas represented by the Baltic and the North seas, this includes many other coastal environments [19], such as the Iberian nearshore [20], the Mediterranean [21] and the Black [22] seas. If the targets set by the European Green Deal in terms of offshore wind can be considered ambitious, those related to the other types of ocean energy are really spectacular. Thus, an increase of more than 3000 times is assumed by 2050 from the currently operating capacity of 13 MW (in 2021). These kinds of marine renewable energy include the floating solar panels [23], which are considered very promising since they are based on a proven technology and can be easily combined with the floating wind. The wave and tide technologies, although are not yet fully mature and economically effective, present the advantage that there are abundant resources, which are more predictable than wind or solar and have a higher power density. In a first approach, collocation with the existent wind energy projects and/or hybrid solutions [24-26] might increase the economic efficiency, especially as regards the wave energy extraction. A solution envisaged to make the marine renewable energy more viable is represented by the Power to X technology. This approach considers hydrogen as an energy vector and in this way the costs of the marine renewable energy may decrease being possible to extract energy in remote locations without a shore connection.

Other kinds of marine renewable energy sources are salinity and thermal gradients that originate from the differences in the salinity and temperature, respectively, of sea water masses. Also, another energy source is represented by the marine biomass energy (marine bioenergy) which involves the use of marine algae and other viable sources for the production of biofuels (i.e., biogas, biodiesel, bioethanol, and other liquid biofuels). Furthermore, another potential marine renewable energy is represented by ocean floor geothermal energy, which considers the use of supercritical geothermal resources in the sea floor.

Finally, it has to be highlighted that the *Journal of Marine Science* represented even from the beginning an open framework dedicated to the presentation of the most significant discoveries and insights in marine science research. Taking into account the high concern of the scientific community related to the climate dynamics, on one hand, and the expected development and very ambitious targets related to the marine renewable energy sector, on the other hand, climate change effects in marine and coastal environment, as well as the assessment of the main challenges and advances associated to the extraction of marine renewable energy are considered topics of extremely high interest for our journal. In this way, we hope that *Journal of Marine Science* will play an active role in following the green road towards a low carbon future.

References

[1] IPCC, 2014. AR5 Synthesis Report: Climate Change 2014. https://www.ipcc.ch/report/ar5/syr/

[2] IPCC, 2021. AR6 Climate Change 2021: The Physical Science Basis. https://www.ipcc.ch/assessment-report/ar6/

[3] Makris, C., Galiatsatou, P., Tolika, K., all, E., 2016. Climate change effects on the marine characteristics of the Aegean and Ionian Seas. Ocean Dynamics. 66, 1603-1635. http://rdcu.be/lL9L

[4] Rusu, E., 2019. A 30-year projection of the future wind energy resources in the coastal environment of the Black Sea. Renewable Energy. 139, 228-234. https://www.sciencedirect.com/science/article/pii/S0960148119302368

[5] Rusu, E., Onea, F., 15 May 2019. An assessment of the wind and wave power potential in the island environment. Energy. 175, 830-846.
DOI: https://doi.org/10.1016/j.energy.2019.03.130

[6] Rusu, E., Onea, F., 2016. Estimation of the wave energy conversion efficiency in the Atlantic Ocean close to the European islands. Renewable Energy. 85, 687-703.
DOI: http://dx.doi.org/10.1016/j.renene.2015.07.042

[7] Rusu, E., Guedes Soares, C., 2012. Wave energy pattern around the Madeira islands. Energy. 5(1), 771-785.
DOI: http://dx.doi.org/10.1016/j.energy.2012.07.013

[8] Rusu, E., Onea, F., 2017. Joint Evaluation of the Wave and Offshore Wind Energy Resources in the Developing Countries. Energies. 10(11), 20.

[9] Rusu, E., Onea, F., December 2019. A parallel evaluation of the wind and wave energy resources along the Latin American and European coastal environ-ments. Renewable Energy. 143, 1594-1607.
DOI: https://doi.org/10.1016/j.renene.2019.05.117

[10] Bento, A.R., Rusu, E., Martinho, P., Guedes Soares, C., 2014. Assessment of the changes induced by a wave energy farm in the nearshore wave conditions. Computers & Geosciences. 71, 50-61.
DOI: http://dx.doi.org/10.1016/j.cageo.2014.03.006

[11] Rusu, E., Onea, F., 2016. Study on the influence of the distance to shore for a wave energy farm operating in the central part of the Portuguese nearshore. Energy Conversion and Management. 114, 209-223.
DOI: http://dx.doi.org/10.1016/j.enconman.2016.02.020

[12] Zanopol, A., Onea, F., Rusu, E., 2014. Coastal impact assessment of a generic wave farm operating in the Romanian nearshore. Energy. 72(8), 652-670. http://www.sciencedirect.com/science/article/pii/S0360544214006604

[13] Rusu, E., Guedes Soares, C., 2013. Coastal impact induced by a Pelamis wave farm operating in the Portuguese nearshore. Renewable Energy. 58, 34-49.
DOI: http://dx.doi.org/10.1016/j.renene.2013.03.001

[14] Raileanu, A., Onea, F., Rusu, E., 2020. An Overview of the Expected Shoreline Impact of the Marine Energy Farms Operating in Different Coastal Environments. J. Mar. Sci. Eng. 8(3), 228.

[15] Onea, F., Rusu, E., 2019. The Expected Shoreline Effect of a Marine Energy Farm Operating Close to Sardinia Island. Water. 11(11), 2303.
DOI: https://doi.org/10.3390/w11112303

[16] Rusu, E., 2020. An evaluation of the wind energy dynamics in the Baltic Sea, past and future projections. Renewable Energy. 160, 350-362.

[17] Rusu, E., Rusu, L., 2021. An evaluation of the wave energy resources in the proximity of the wind farms operating in the North Sea, Energy Reports. 7(3) 19-27. https://www.sciencedirect.com/science/article/pii/S2352484721003474

[18] European Commission, 2019. Communication on the European Green Deal https://ec.europa.eu/info/publications/communication-european-green-deal_en

[19] Raileanu, A.B., Onea, F., Rusu, E., 2015. Evaluation of the offshore wind resources in the European seas based on satellite measurements. Energy and Clean Technologies. 227-234.

[20] Ruiz, A., Onea, F., Rusu, E., 2020. Study Concerning the Expected Dynamics of the Wind Energy Resources in the Iberian Nearshore. Energies. 13(18), 4832.

[21] Onea, F., Deleanu, L., Rusu, L., Georgescu, C., 2016. Evaluation of the wind energy potential along the Mediterranean Sea coasts. Energy Exploration & Ex-

ploitation. 34(5), 766-792.

[22] Onea, F., Rusu, E., 2016. Efficiency assessments for some state of the art wind turbines in the coastal environments of the Black and the Caspian seas. Energy Exploration & Exploitation. 34(2), 217-234.

[23] Ravichandran, N., Fayek, H., Rusu, E., 2021. Emerging Floating Photovoltaic System—Case Studies High Dam and Aswan Reservoir in Egypt. Processes. 9(6), 1005.
DOI: https://doi.org/10.3390/pr9061005

[24] Onea, F., Ciortan, S., Rusu, E., 2017. Assessment of the potential for developing combined wind-wave projects in the European nearshore. Energy & Environment. 28(5-6), 580-597.

[25] Onea, F., Rusu, E., 2016. The expected efficiency and coastal impact of a hybrid energy farm operating in the Portuguese nearshore. Energy. 97, 411-423.

[26] Rusu, E., Onea, F., 2017. Hybrid Solutions for Energy Extraction in Coastal Environment. Energy Procedia.
DOI: https://doi.org/10.1016/j.egypro.2017.07.

About the Publisher

Bilingual Publishing Co. (BPC) is an international publisher of online, open access and scholarly peer-reviewed journals covering a wide range of academic disciplines including science, technology, medicine, engineering, education and social science. Reflecting the latest research from a broad sweep of subjects, our content is accessible world-wide——both in print and online.

BPC aims to provide an analytics as well as platform for information exchange and discussion that help organizations and professionals in advancing society for the betterment of mankind. BPC hopes to be indexed by well-known databases in order to expand its reach to the science community, and eventually grow to be a reputable publisher recognized by scholars and researchers around the world.

BPC adopts the Open Journal Systems, see on ojs.bilpublishing.com

Database Inclusion

Asia & Pacific Science
Citation Index

Creative Commons

China National Knowledge
Infrastructure

Google Scholar

Crossref

MyScienceWork